ISTITUTO NAZIONALE DI FISICA NUCLEARE
Laboratori Nazionali di Frascati

LNF-78/48

A. Małecki, J. M. Namysłowski, A. Reale and B. Minetti :
HEAVY-ION COLLISIONS AT INTERMEDIATE ENERGIES: ELASTIC SCATTERING, COULOMB EXCITATION AND NUCLEON TRANSFER REACTION.

Estratto da :
Riv. Nuovo Cimento 1 (10), 1 (1978).

Servizio Documentazione
dei Laboratori Nazionali di Frascati
Cas. Postale 13 - Frascati (Roma)

A. Małecki, J. M. Namysłowski, A. Reale and B. Minetti

Heavy-Ion Collisions at Intermediate Energies: Elastic Scattering, Coulomb Excitation and Nucleon Transfer Reaction.

RIVISTA DEL NUOVO CIMENTO VOL. 1, N. 10 1978

Heavy-Ion Collisions at Intermediate Energies: Elastic Scattering, Coulomb Excitation and Nucleon Transfer Reaction.

A. MAŁECKI

Institute of Nuclear Physics - Cracow, Poland

J. M. NAMYSŁOWSKI

Institute of Theoretical Physics, Warsawa University - Warsawa, Poland

A. REALE

Istituto Nazionale di Fisica Nucleare, Laboratori Nazionali - Frascati, Italia

B. MINETTI

Istituto di Fisica Sperimentale del Politecnico - Torino, Italia

(ricevuto il 9 Maggio 1977)

CHAPTER 1

The outlook of interest in heavy-ion collisions.

1.1. – Introductory remarks.

There are several reasons why one wants to scatter heavy ions, in spite of their complicated structure. Before describing them let us, however, make some introductory remarks concerning the characteristic features of heavy-ion collisions.

The most important property is the smallness of the wave-length λ in the relative motion of two heavy ions; λ is small in comparison with the characteristic distance D. The ratio λ/D is of the order 10^{-2}. Small λ makes it reasonable to talk about the Newton trajectories. Ions moving on these trajectories are repelled from each other by strong Coulomb field, and for not too high energies we can introduce the notion of a distance of closest approach in a head-on collision for the backward scattering. We denote this distance by $2a$, and illustrate it in fig. 1.1.

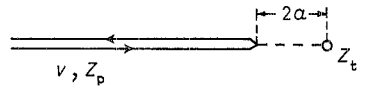

Fig. 1.1. – Projectile Z_p approaching the target Z_t with the relative velocity v moving in a head-on collision.

From the Newton law we get

$$a = \frac{Z_p Z_t e^2}{\mu v^2}, \tag{1.1}$$

where μ is the reduced mass of two ions.

Taking the ratio of a to $\lambda = \hbar(\mu v)^{-1}$, we get ($\beta = v/c$)

$$\frac{a}{\lambda} = \eta = \frac{Z_p Z_t e^2}{\hbar v} = \frac{Z_p Z_t}{137\beta} \tag{1.2}$$

This ratio η is an important, large, dimensionless parameter and it enters the well-known formula for the Rutherford scattering cross-section in the following way:

$$\left(\frac{d\sigma}{d\Omega}\right)_{\text{Ruth}} = \frac{1}{4}\eta^2(\mu v)^{-2}\sin^{-4}\frac{\theta}{2}. \tag{1.3}$$

Varying the laboratory energy of the projectile ion, one gets to the so-called Coulomb barrier, which is the maximum safe bombarding energy before we enter the field of nuclear force. Denoting the Coulomb barrier by E_{CB}, we get an expression for it by equating the centre-of-mass relative-motion energy with the electrostatic energy at the distance of closest approach:

$$E_{\mathrm{CB}}\left(1+\frac{A_1}{A_2}\right)^{-1} = Z_1 Z_2 e^2 (R_1 + R_2 + \Delta)^{-1}\,, \tag{1.4}$$

where A, Z, R are ion mass number, charge and radius, respectively, and $\Delta \approx 3$ fm. Taking $R = 1.41\ A^{\frac{1}{3}}$, $Z \approx 0.49\ A(1 + A^{\frac{2}{3}}(166)^{-1})^{-1}$, we get in fig. 1.2 the plot of the Coulomb barrier E_{CB}, in MeV for different charges of projectile, as a function of the charge of the target.

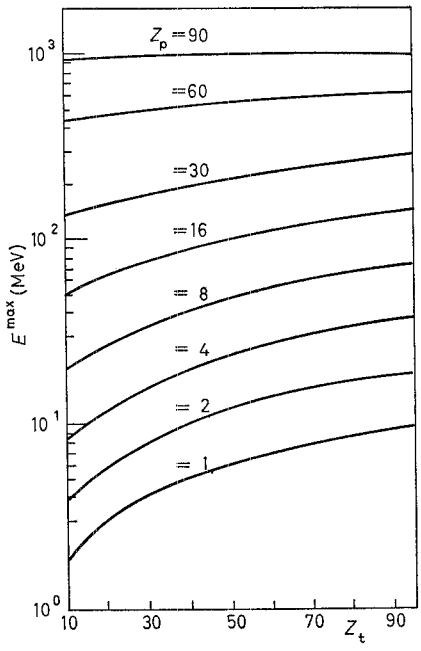

Fig. 1.2. – The maximal bombarding energy E_{CB} is shown as a function of the target charge Z_t for different projectiles Z_p. From ref. [1.1].

For energies below the Coulomb barrier ions are strongly repelled by the Coulomb force, while for energies above the Coulomb barrier there is a strong absorption at very small distances which also prevents us to see such final ions which deeply penetrated one into the other. Therefore, the heavy-ion collision is a peripheral, or surface process, and a typical distance D which characterizes the smallest interesting distance above the Coulomb barrier is

roughly the sum of the two radii of the ions. For an arbitrary energy, the definition of D is

$$D = \begin{cases} 2a & \text{for } E < E_{\text{CB}}\,, \\ R_1 + R_2 & \text{for } E > E_{\text{CB}}\,. \end{cases} \tag{1.5}$$

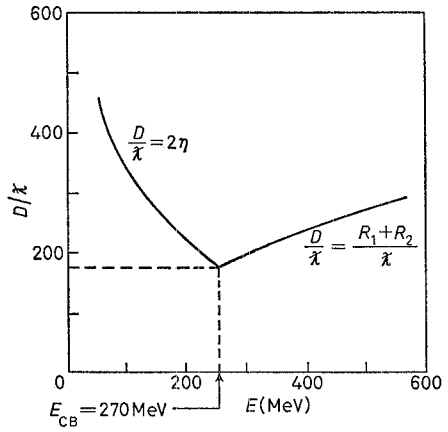

Fig. 1.3. – The ratio between the characteristic D and the wave-lenght in the relative motion for argon projectiles on mercury as a function of bombarding energy in MeV. For energies below the Coulomb barrier ($E_{\text{CB}} \approx 270$ MeV), D is taken to be the distance of closest approach in a head-on collision, while, for $E > E_{\text{CB}}$, D is taken to be the sum of the nuclear radii. From ref. [1.2].

As an example we show in fig. 1.3 the large dimensioneless parameter $D \cdot \lambda\!\!\!^{-}^{-1}$ for scattering of argon on mercury as a function of the projectile energy.

The fact that $D \cdot \lambda\!\!\!^{-}^{-1}$ is very large ($\geqslant 200$) implies that the semi-classical, WKB or eikonal descriptions have a very good chance to work well. These simple methods, which yield the analytic or almost analytic form of expressions for the cross-sections, constitute the basic framework for the study of dynamics in the heavy-ion collisions.

1.2. – Outlook of interest in heavy-ion collisions.

The present-day experiments with heavy-ion beams are done either below the Coulomb barrier or just above it, around 10 MeV/nucleon, or at much higher energies from about 200 MeV/nucleon up to 2000 MeV/nucleon. The intermediate energy region in the gap from 10 MeV/nucleon to 150 MeV/nucleon is such that different phenomena will manifest themselves in this energy range and for illustration we reproduce in fig. 1.4 a drawing made by SWIATECKI [1.3]. We note that in the gap region nuclear physics will be studied under some special compressed conditions, and that it will get overlapped with the meson

physics. Studying heavy-ion physics in this range of energy, one would also aim at a common view on heavy-ion processes in the low, intermediate and high energies. This requires to focus our attention both on the conventional heavy-ion processes met in the low energies and on the new phenomena.

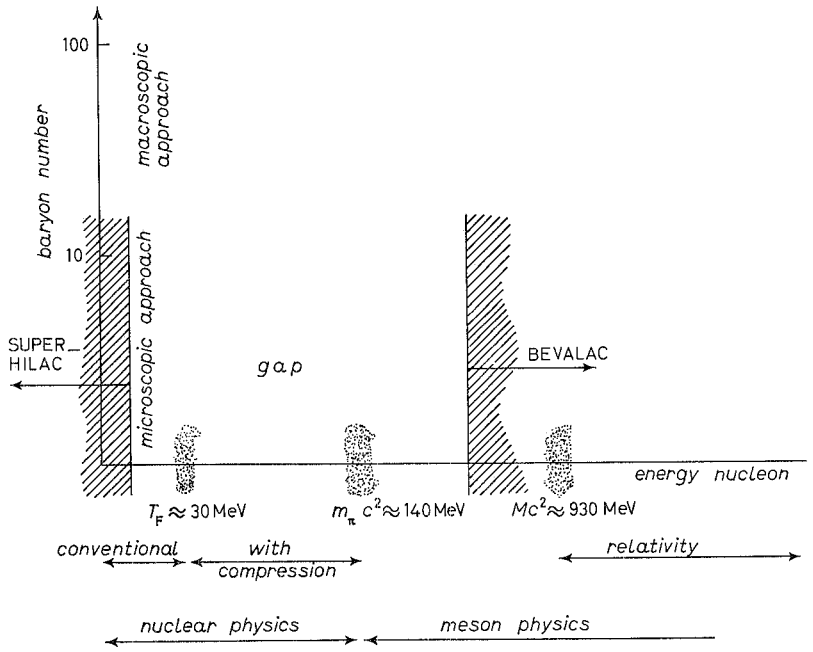

Fig. 1.4. – From ref. [1.3].

We may distinguish three energy regions where the reasons of scientific interest are somewhat different:

A) *Phenomena below the Coulomb barrier* [1.4]. – Below the Coulomb barrier the heavy-ion interaction is essentially of the electromagnetic type and it is known. Therefore, such processes as the Coulomb excitation [1.4] and the so-called sub-Coulomb transfer reactions [1.14] attract most of the attention. With a good precision one can find spectroscopic factors, since in this energy range the Coulomb wave functions are excellent approximations to the full scattering wave functions.

The strong Coulomb field between the heavy ions is also advantageous for other reasons. It can excite high-spin states, or it can make possible the fission of nuclei (Coulomb fission). Because of the strong Coulomb field, which even sometimes can become supercritical, it is interesting to make a precise measurement of the elastic scattering, since we can look for delicate modifications of the ordinary QED effects.

During the time of collision of two heavy ions a superheavy molecule can emerge. In such a molecule, the electron feels attraction coming from both ions and, in the case of a supercritical Coulomb field, it must coexist with the sea of positrons. Vacuum gets polarized, and one can study the X-ray spectroscopy for the superheavy molecule, learning new aspects of QED in the very strong Coulomb fields.

B) *Phenomena above the Coulomb barrier.* – In this energy region we can study

1) the mechanism of the elastic scattering, inelastic excitation of the residual nucleus and transfer reactions,

2) the nuclear spectroscopy, by either combining it with the mechanism of nuclear reactions and studying spectroscopic factors and deep inelastic processes, or looking at the composite systems by studying the γ-spectroscopy of the high-spin states, complete fusion and departures off the stability line.

B.1. Elastic scattering [1.5], transfer reactions [1.6] and inelastic excitations. These topics shall be elaborated in detail in chapters 3, 4 and 5, after presentation of the experimental facilities in chapter 2. Chapters 2 and 3 serve as an introduction to the subject. The main body of the paper are chapters 4 and 5. In them we emphasize the eikonal methods for dealing with the elastic scattering, inelastic excitations and transfer reactions, since we feel that they can provide us with a uniform way of interpreting the data at different energies, particularly at the intermediate and high energies, *i.e.* including the « gap » and the Bevalac regions in fig. 1.4.

B.2.1. Spectroscopic factors. – Increasing the energy of the projectile above the Coulomb barrier we allow for a complicated interplay of the Coulomb and nuclear forces, and necessarily the formalism becomes more involved than in the sub-Coulomb region. However, the cross-section for the transfer reactions increases. Kinematical selection rules favour large angular-momentum transfer, and large cross-section enables us to reach nuclear states with high spin, which are difficult to populate otherwise. In fact, at energies around 10 MeV/nucleon there was noted high selectivity to high-spin states [1.7].

B.2.2. Deep inelastic processes. – When two nuclei do not reach some characteristic distance, then the complete fusion cannot be obtained. If a projectile is not completely absorbed, it can lose kinetic energy, or it can lose or gain electric charge and mass. The projectile which is slowed down in such a way will leave the collision region not in consequence of the initial momentum but because of the Coulomb repulsion. These « deep inelastic processes » are sometimes called strongly damped collisions because of the strong damping of the energy degrees of freedom. In the exit channel a large amount of energy is converted into the excitation energy. HUIZENGA [1.9] gives the following characteristics

of the strongly damped collisions: 1) the exit fragments have generally masses not far from the masses of projectile and target, although, if the target mass is large enough, the excited heavy fragment will sequentially fission; 2) the kinetic energies of fragments correspond to Coulomb energies for charge centres of highly deformed fragments, analogous to that for fission fragments; 3) the angular distributions are strongly peaked, as in the direct processes. The cross-section for these processes may be a major part of the total cross-section at intermediate energies.

B.2.3. γ-spectroscopy and the behaviour of high-spin states. – The products of heavy-ion collisions can acquire very large angular momenta, up to 100 units of $\hbar$. These objects, after evaporating a few neutrons, send out cascades of γ-rays, which can be used to learn about the properties of very-high-spin states. The nuclear systems « rotating » with very large spins are put under extreme conditions. The nuclear-structure studies have to be extended to this entirely new regime, since the change of the nuclear structure may be very drastic [1.8].

B.2.4. Complete fusion. – The high rotation energy can produce great deformation of a nucleus and will increase its tendency to fissioning. This tendency depends also on the momentum of inertia of nucleus. One can ask the question whether the high angular momentum does not preclude the existence of the fusion nucleus. In this respect it is important to explore the so-called « yrast » line. When a nucleus is in the « yrast » state, all the excitation energy E is in the rotational energy. The « yrast » line $E = E(J)$ by definition precludes the existence of an excited state of spin J below it. The shape of the « yrast » line depends on the properties of the excited nucleus and its knowledge is of great interest.

B.2.5. Departure off the stability line. – Another area of the nuclear-structure study with heavy ions is the search for the properties of nuclides far off the stability line. The large excess of neutrons, which can be found in the products of heavy-ion collisions, enable us to get extra conditions for the nuclear-structure models of the stable nuclei. The outcoming nuclei can carry out in a more or less stable way a great number of neutrons or protons, so that one can hope to study new nuclei. This has been already done at Dubna, where many new isotopes have been observed, like $^{24}_{8}O$, by bombarding heavy-ion targets with O, Ne, Ar at (10÷15) MeV/nucleon and observing that the outcoming projectile was enriched in neutrons.

C) *Phenomena much above the Coulomb barrier.* – We shall here restrict ourselves to only nuclear fragmentation and the so-called unusual phenomena, which include the nuclear shock waves, and the supercritical Coulomb and pion fields. It is also possible that the phenomena of the deep inelastic collisions, mentioned in subsect. *B*.2.2, play a very important role in the energy

range much above the Coulomb barrier, which approximately can be defined as starting from an energy higher by about an order of magnitude than the Coulomb barrier.

C.1. Nuclear fragmentation. The fragmentation of a nucleus in nuclear collisions seems to be an interesting problem not only at relativistic energies, but also around (100÷200) MeV per nucleon. Some results indicate [1.10] that the fragmentation cross-section is independent of energy in a large range from 0.1 to 2.0 GeV/nucleon, which is surprising and deserves further studies.

C.2. Unusual processes. During the collision of a high-energetic nucleus with a heavy target a high-density, supersonic compression wave (shock waves) may be generated [1.11]. The high temperature reached in the shock zone allows for the creation of nucleon isobars, and the strong pion field (supercritical meson field) can manifest itself in the pionization and the appearance of pion condensate, which is the macroscopic population of a low-frequency pion field. The meson production renders the hadronic matter less « stiff », so that great compression can be attained. The very dense, hot, highly isobaric nuclear matter with « layers » of pions condensated, which occur in the shock zones, has quite different properties than the normal nuclear matter [1.12, 1.15].

The unusual situation appears also for QED if the sum of the projectile and target charges exceeds about 172 [1.13]. Vacuum gets polarized and decays, emitting positrons and letting the very strongly bound electron with the binding energy in the vicinity of two rest masses to become an unbound state, of a resonance character, co-existing with the sea of positrons. The physical vacuum, in the sense of the lowest energy state, becomes charged and we find an example of the spontaneously broken symmetry. The last phenomenon is also met in the currently discussed unified theories of weak and electromagnetic interactions. It is notable that the study of heavy-ion collisions may shed some light on the fundamental question of the interaction of elementary particles and even on models of them [1.16]. The models of elementary particles, considered as bags of quarks, may in turn be useful in discussing the central high-energy collisions of heavy ions.

REFERENCES

[1.1] K. ADLER: in *Oak Ridge Heavy-Ion Summer Study*, edited by S. T. THORNTON (Oak Ridge, Tenn., 1972).
[1.2] R. A. BROGLIA and A. WINTHER: *Phys. Rep.*, **4** C, 153 (1972).
[1.3] W. J. SWIATECKI: in *II High-Energy Heavy-Ion Summer Study, July 1974*, Report LBL-3675 (1974), p. 349.

[1.4] K. ALDER and A. WINTHER: *Coulomb Excitation. A Collection of Reprints with an Introductory Review* (New York, N. Y., 1966).
[1.5] T. W. DONNELLY, J. DUBACH and J. D. WALECKA: *Nucl. Phys.*, **232** A, 355 (1974); A. DAR and Z. KIRZON: *Nucl. Phys.*, **237** A, 319 (1975).
[1.6] *Symposium on Heavy-Ion Transfer Reactions, Argonne, 1973*, Report PHY-1973B (1973).
[1.7] N. ANYAS-WEISS, J. C. CORNELL, P. S. FISHER, P. N. HUDSON, A. MENCHACA-ROCHA, D. J. MILLENER, A. D. PANAGIOTOU, D. K. SCOTT, D. STROTTMAN, D. M. BRINK and B. BUCK: *Phys. Rep.*, **12** C, 203 (1974).
[1.8] Z. SZYMANSKI: in *Proceedings of the International Conference on Nuclear Physics, Munich, 1973*, edited by J. DE BOER and H. J. MANG (Amsterdam, 1973), p. 402.
[1.9] N. HUIZENGA: in *Proceedings of the VII Masurian School in Nuclear Physics, Nukleonika*, **20**, 291 (1975); *Phys. Rev. C*, **11**, 1265 (1975).
[1.10] K. KRISTIANSSON, R. KULLBERG, B. LINQKVIST and I. OTTERLUND: in *Proceedings of the XIV International Cosmic-Ray Conference*, Vol. 7 (Munich, 1975), p. 2358.
[1.11] H. G. BAUMGARDT, J. U. SCHOTT, Y. SAKAMOTO, E. SCHOPPER, H. STÖCKER, J. HOFMAN, W. SCHEID and W. GREINER: *Zeits. Phys.*, **273** A, 359 (1975).
[1.12] T. D. LEE and G. C. WICK: *Phys. Rev. D*, **9**, 2291 (1974).
[1.13] B. MÜLLER, H. PEITZ, J. RAFELSKI and W. GREINER: *Phys. Rev. Lett.*, **28**, 1235 (1972).
[1.14] G. BAUER and G. TRAUTMANN: *Phys. Lett.*, **25** C, 294 (1976).
[1.15] J. M. NAMYSLOWSKI: in *Proceedings of the VIII Masurian School in Nuclear Physics, Nucleonika* (1977).
[1.16] P. E. HODGSON: *Riv. Nuovo Cimento*, **1**, No. 1 (1978).

CHAPTER 2

Heavy-ion accelerating machines and experimental facilities.

2.1. – Heavy-ion machines.

In these years the various scientific communities have considered with great interest the convenience of building heavy-ion accelerating machines. The main purpose is to get heavy-ion beams of great intensity and high energy.

It is well known that the usual electrostatic accelerators have already provided a great deal of information on the structure of nuclei, but they are strongly limited to energies either below or just above the Coulombian barrier. On the other hand, high-energy accelerators like the Bevalac are limited to very high relativistic energies, say $(2500 \div 250)$ MeV/nucleon so that intermediate energies are actually not covered by the existing machines. This is a great disadvantage for our knowledge of nuclear matter, because many interesting phenomena are expected in that region [2.1]. This limitation will be overcome by the future machines so that the way is open to new discoveries in the field of nuclear physics.

Of course the « ideal » heavy-ion accelerating machine should be able to give ion beams of all nuclear species from H to U, of great intensities, say $> 10^{11}$ particles/s in a wide energy range from ~ 1 MeV/nucleon to $\sim 10^4$ MeV/nucleon with a very good energy resolution and possibly long duty cycles to perform coincidence experiments. As matter of fact, in order to avoid increasing too much the financial efforts and the technical difficulties, each laboratory is forced to plan the construction of a specific machine, which will allow us to do physics in some specific energy range or with some restriction on the kind of projectiles.

What kind of machine is then more convenient depends on the physical interest; *e.g.* low-energy very intense beams are needed to look at excitation levels of nuclei, while one has to use relativistic-energy beams to study, say, the nuclear fragmentation phenomena.

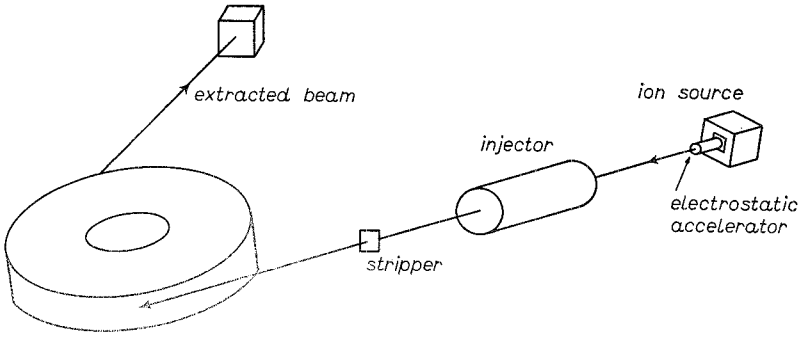

Fig. 2.1. – Schematic layout of an heavy-ion circular accelerator.

The general way of obtaining ion beams is sketched in fig. 2.1 for circular accelerators.

As is shown, charged atoms coming from the source are injected in some kind of preaccelerator which can be of an electrostatic type (Van der Graaff, Tandem) or a Linac or a small cyclotron or both. Depending on the type of injector, the ions sources have to produce either negative-ion beams (Heinicke sources, duoplasmatron, etc.), *i.e.* atoms to which an electron has been « added » (as for a Tandem), or positively charged ions (Penning sources), *i.e.* atoms which have been spoiled (stripped) of one or more orbital electrons (as for cyclotrons or Linac injectors).

Usually ions, after having been accelerated to some energy by the injector, are again stripped in T (by making them traverse a very thin foil of material), so that their final effective charge is $\bar{Z} \leqslant Z$. After the second stripping, they are injected into the circular ring and accelerated, by a suitable system of accelerating cavities or in some other way, to achieve the final energy. In

the usual cyclotrons or synchrotrons the final energy per nucleon is given by

$$\varepsilon_t = \frac{E_t}{A} = KB^2R^2\left(\frac{\bar{Z}}{A}\right)^2,$$

where K is some numerical factor, B and R are the magnetic field and the magnetic radius of the machine, respectively.

One can see from the previous formula the convenience of obtaining ionized atoms of great $\bar{Z}$ in order to arrive at high final energies. Unfortunately, there are some limitations of the charge state $\bar{Z}$ that one can get from the sources or in the stripping process; the difficulties are greater for heavier atoms. Of course it would be the best to have fully ionized atoms, but this is not so easy because the ionization efficiency in the stripping process in T is limited depending on the ion energy at the output of the injector and on the considered nucleus.

The average charge state $\bar{Z}$ depends, in fact, on the nucleus energy according to the formula [2.2]

$$Z = c\sqrt{Z\cdot\varepsilon_{\text{inj}}}, \qquad 0.1 < \frac{\bar{Z}}{A} < 0.4,$$

where c is a numerical constant depending on whether the stripper is a solid or a gaseous target, and Z and ε_{inj} are the atomic number and energy/nucleon at the output of the injector, respectively. One can see that high-energy injectors would be convenient to reach high ionization states $\bar{Z}$, but they are of course too much expensive.

It is not so difficult to have light nuclei fully stripped ($\bar{Z} = Z$), but for heavier nuclei $\bar{Z}$ is usually less than Z.

For what concerns the intensities of the output beams, these of course depend on the features of the ion sources, the injector and final acceptances, the possibility of producing a good vacuum (better than 10^{-8} mm Hg) inside the circular rings, which is relevant to a good transmission during the acceleration cycle, stripper efficiency and so on. A great technical progress is expected in the next years in the heavy-ion performances both of negative- and of positive-ion sources.

For the sake of clarity it is convenient to divide the new accelerator projects into three classes:

a) New electrostatic accelerators, which can give very intense ion beams, of low energy/nucleon say $E/A \leqslant 10$ MeV/nucleon, but of very great energy resolution. The intensity of the outcoming beams from these machines is greater than 10^{12} particles/s and the energy resolution is of the order of 10^{-4}. The usual Van de Graaff or Tandem generators are working in this way.

b) Cyclotrons or Linac accelerators are meant to be useful for getting very intense beams ($\geqslant 10^{11}$ particles/s) within an energy range of, say, (10 ÷ 100) MeV/nucleon.

TABLE 2.I.

Type of machine	Site	MeV/nucleon	Nuclei	Status
s.c. Linac	Argonne, Karlsrue	$\leqslant 10$	$\rightarrow$ U	proposed
Superhilac	Berkeley	8.5	$\rightarrow$ U	OK
Unilac	Darmstadt	$30 \div 8$	$\rightarrow$ U	1975 start
Bevalac	Berkeley	$2500 \div 250$	$\rightarrow$ Ne	1974 start
Saturne II	Saclay	$2000 \div 200$		construction
Ganil	Caen	$100 \div 10$	$\rightarrow$ U	construction
Alice (cyclotron+Linac)	Orsay	$\leqslant 5$	$\rightarrow$ Kr	OK
Cyclotron U-300	Dubna	~ 10	$\rightarrow$ Zn	OK
Cyclotron U-300+U-200	Dubna	~ 7	$\rightarrow$ Xe	OK
Cyclotron U 400		~ 10	$\rightarrow$ U	constructed
		50	$\rightarrow$ Ne	
Cyclotron U 200	Warsaw	20	$\rightarrow$ A	constructed
Cyclotron	Oak Ridge	$100 \div 10$		proposed
s.c. Cyclotron	Italy	$55 \div 10$	$\rightarrow$ U	proposed
s.c. Cyclotron	Chalk River	$50 \div 10$	$\rightarrow$ U	proposed
s.c. Cyclotron	Michigan	$50 \div 10$	$\rightarrow$ U	proposed
Tandem	USA	13 (MV)		
Tandem	France	13 (MV)		
Tandem	Netherland	13 (MV)		
Tandem	Denmark	13 (MV)		
Tandem	Germany	13 (MV)		
Tandem	England	$\geqslant 30$ (MV)		
Tandem	Rumania	10 (MV)		
Tandem	Italy (Legnaro)	16 (MV)		
Tandem	Italy (Catania)	13 (MV)		
Pelletron	Australia	14 (MV)		
Pelletron	Israel	14 (MV)		
Pelletron	Brasil	12 (MV)		
Accelerator facilities in Japan (Tandem+Linac+synchrotron)	Japan	$10 \div 500$	$\rightarrow$ U	constructed
Cyclotron Virksi-s.c. Cyclotron	Berlin	8	$\rightarrow$ Fe	constructed

c) Circular machines, like synchrotrons, which can give high-energy beams, say (100 ÷ 3000) MeV/nucleon with typical intensities $\leqslant 10^{10}$ particles/s.

The construction of all the devices is achieved either by constructing *ex novo* the machines or by conversion of machines already existing. As we said, the main difficulty of all these projects is to balance the financial difficulties with the goal of high-energy–high-intensity ion beams.

Among the various existing projects, one could mention as examples of the type-*b*) projects the French national project GANIL, the UNILAC of Darmstadt, the Japanese NUMITRON and in Italy the project of a superconducting cyclotron [2.4].

One has to consider as projects of type *c*) the Bevalac of the Berkeley Laboratories, the AGS of Brookhaven, the French Saturne II and probably the Serpukov protosynchrotron [2.5]. Few years ago in Frascati the proposal has also been made of converting the 1.1 GeV electronsynchrotron into an ion

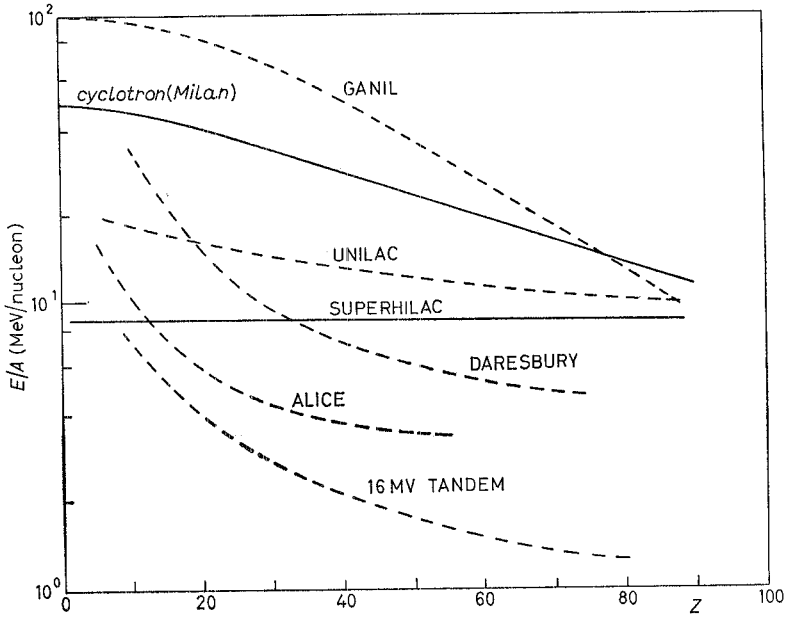

Fig. 2.2. – Energy/nucleons atomic number for different heavy-ion machines.

accelerator [2.6]. In fig. 2.2 we report a graph of the energies of some projects, while in tables 2.I and 2.II we tried to summarize the world situation concerning most of the projects.

It is worthwhile writing as in table 2.III the gross features of the beams coming out from few ones of the considered circular accelerators, in order to give the relevant information for planning future experiments.

TABLE 2.II.

	Tandem	Linac	Cyclotron and synchrotron
E/A	$\leqslant 10$ MeV/nucleon	~ 10 MeV/nucleon	$\sim (100 \div 2500)$ MeV/nucleon
Z	any	$\sim$ any	$\sim$ any
Intensity	μA or fraction of μA	$(10 \div 100)\ \mu$A	$(10^9 \div 10^{12})$ p/s
Duty cycle	1	$(20 \div 100)\%$	$(10 \div 20)\%$
$\Delta p/p$	$< 10^{-4}$	$(0.3 \div 1)\%$	$(0.1 \div 0.5)\%$

TABLE 2.III.

Project	Energy/nucleon (approx.) (MeV/nucleon)	Nuclei	Intensity (pps)	Beam energy resolution
Superconducting cyclotron (Milan)	$55 \div 10$	He → U	$\sim 10^{11}$	0.1%
GANIL	$100 \div 10$	He → U	$\sim 10^{12}$	0.1%
UNILAC	$30 \div 8$	He → U	$\geqslant 10^{12}$	0.25%
Saturne II	$2000 \div 200$	He → Ne	$10^9 \div 10^{10}$	0.3%
U-400 (Warsaw)	$20 \div 7$	He → U	$10^{12} \div 10^{13}$	0.4%

As one can see from table 2.I, one can expect that in the next years there will be available very intense ion beams of all possible energies between few MeV/nucleon up to 10^4 MeV/nucleon with an energy resolution of $(0.1 \div 0.2)\%$ and very good optical properties.

2.2. – Experimental facilities.

To perform an experimental program concerning the phenomena we discussed in sect. **1.2**, we have to provide a suitable experimental apparatus for measuring angular and energy distributions of the emitted particles and their mass numbers, at different projectile energies (we refer to BRESSANI [2.3] for a more detailed analysis).

Let us consider first two-body elastic or inelastic reactions at energies of the projectile nuclei around 100 MeV/nucleon:

$$A + B \rightarrow C + D\,. \tag{2.1}$$

Rates for reactions (2.1) depend on many factors as beam intensity, target thickness, angular acceptance of the experimental apparatus and, of course, the cross-section of the considered processes at these energies. One cannot increase too much the useful target thickness, in order to limit energy losses and Coulombian scattering of the emitted particles in the target. Generally an acceptable value for the target thickness is in the range $(0.2 \div 2)$ mg/cm^2. In these conditions at least for lighter ions the momentum resolution will be comparable with the momentum resolution of the incoming beam reported in table 2.IV.

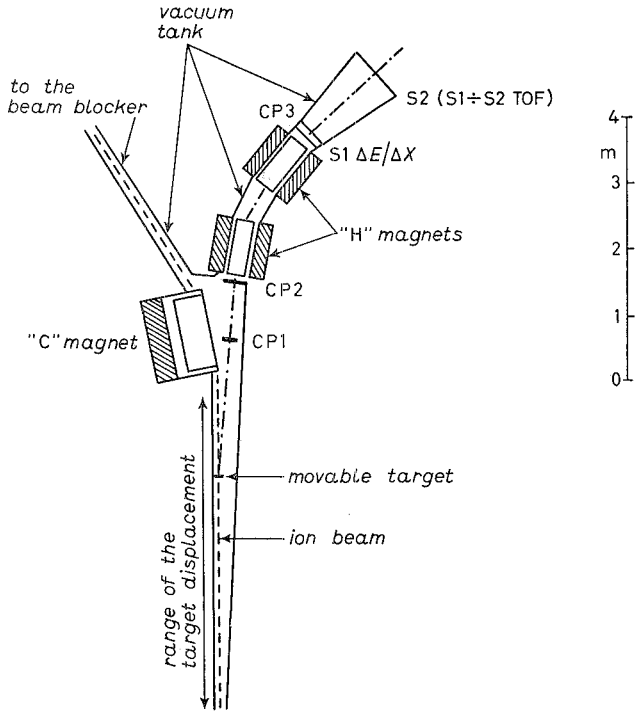

Fig. 2.3. – General layout of an experimental apparatus for heavy-ion two-body reactions (from ref. [2.3]).

It is in fact necessary to have an experimental apparatus with good angular and energy resolution to allow the measurement of many of the reactions we have listed in sect. **1.2**. For the two-body reaction an experimental apparatus like the Saclay energy loss spectrometer [2.7], that has an energy resolution of ~ 100 keV, would be fully adequate for most of the reactions we mentioned, apart from its high cost. Of course one has also to consider less expensive experimental solutions like the so-called Palevsky spectrometer [2.8] in some modified version as the one of ref. [2.3] that is reported in fig. 2.3. As one can see

from fig. 2.3, the magnet C is necessary to bend the primary beam, while the two H magnets are used to analyse the emitted particles. The trajectories of the particles in the spectrometer are measured by a system of multiwire proportional chambers or drift chambers. The emission angle of the emitted particles can be varied by a displacement of the target along the beam direction of motion and by keeping the position of the spectrometer fixed.

With such a system one can show [2.3] that energy and angular resolution can be obtained of the order of

$$\delta E/E \simeq \pm 0.3\,\%, \qquad \delta\theta \simeq \pm 2 \text{ mrad},$$

in an angular interval between say 4° and 20° (laboratory system) with a spectrometer acceptance of the order of $(1 \div 2) \cdot 10^{-3}$ sr and a momentum acceptance of ~ 20 MeV/c.

A typical value of the involved momentum is

$$p \simeq 7 \text{ GeV/c} \qquad \text{for the } {}^{16}\text{O nucleus with } E/A = 100 \text{ MeV/nucleon}.$$

As an example of the expected distribution we quote from ref. [4.2] a typical elastic-scattering spectrum of ^{16}O or ^{12}C at $E_{\text{lab}} = 163$ MeV that is at about 10 MeV/nucleon in the laboratory system (see fig. 4.8).

For studying many-body reactions like

$$\text{A}+\text{B} \rightarrow \text{C}+\text{D}+\text{E}+ \ldots$$

in this energy range one can think about experimental devices which are typicla of high-energy particle experiments. There are mainly MWPC and scintillator arrangements, in a closed or open configuration around the target, to get the emission angles and energies of the emitted particles, their specific energy loss $\mathrm{d}E/\mathrm{d}x$ and times of flight. Of course for some type of reactions it is also necessary to try to reconstruct also the masses of the emitted particles. For light ions a complete mass separation is possible [2.4], for heavier ions it is more difficult and single reactions should be examinated separately.

REFERENCES

[2.1] *II High-Energy Heavy-Ion Summer Study*, Lawrence Berkeley Laboratory (July 1974).

[2.2] CH. SCHMELZER: in *Linear Accelerators*, edited by P. M. LAPOSTOLLE and A. L. SEPTIER, p. 1036.

[2.3] M. BASSETTI, U. BIZZARRI, G. BRAUTTI, T. BRESSANI, A. CATTONI, V. CHIMENTI, E. IAROCCI, T. LETARDI, F. LUCCI, A. LUCCIO, G. MAGGIPINTO, C. MARTUSCELLI, C. MENCUCCINI, A. PANTALEO, M. PELLICCIONI, M. PREGER, A. RAINÒ, A. REALE, A. RENIERI, M. SASSI, R. SCRIMAGLIO, S. TAZZARI, F. TAZZIOLI and A. TURRIN: *Conversione dell'elettrosincrotrone dei Laboratori Nazionali di Frascati in acceleratore di ioni*, Rapporto dei LNF (1975).

[2.4] GANIL, *Rapport du group de travail pour l'Accelerateur National a Ion Lourds* (1973); E. ACERBI, G. BACCAGLIONI, G. BELLOMO, C. BIRATTARI, M. CASTIGLIONI, C. DE MARTINO, E. FABRICI, L. GRILLO, S. MICHELETTI, C. PAGANI, M. PIGNANELLI, F. RESMINI and G. TAGLIAFERRI: *Studio del progetto di un ciclotrone superconduttore per ioni pesanti*, Istituto Nazionale di Fisica Nucleare, Sezione di Milano (1976).

[2.5] *Proposal 32: High-intensity uranium beams from the Superhilac and the Bevalac*, Lawrence Berkeley Laboratory; *Proposal of conversion of the Brookhaven AFS into an ion accelerator, Report Interet des Ions lourds relativistes à Saturne II*, Saturne II Entreprise commune CEA 1N2P3, report interne (1975).

[2.6] G. BRAUTTI: *Convertibilità dell'elettrosincrotrone di Frascati per l'accelerazione di ioni*, Rapporto dell'Istituto di Fisica dell'Università, Bari, e Istituto Nazionale di Fisica Nucleare, Sottosezione di Bari (1972); G. BRAUTTI, T. LETARDI, G. MAGGIPINTO and A. REALE: *Il sincrotrone di Frascati come acceleratore di ioni: modifiche strutturali e programmi, Possibili sviluppi del progetto, presentato al Convegno del 16-17 Maggio 1974 in Frascati*, Rapporto LNF-74/49 (1974).

[2.7] J. THIRION: *Proceedings of the International Conference on Nuclear Physics, Munich, 1973*, edited by J. DE BOER and H. J. MANG (Amsterdam, 1973), p. 781.

[2.8] J. L. FRIEDES, R. SUTTER, H. PALEVSKY, G. BENNET, G. IGO, W. D. SIMPSON, R. L. STEARMS and D. M. CORLEY: *Nucl. Instr. Meth.*, **54**, 1 (1967); R. J. SUTTER, G. BENNET, J. FISHER, J. L. FRIEDES, H. PALEVSKY, R. PERSSON, G. IGO and W. D. SIMPSON: *Nucl. Instr. Meth.*, **54**, 71 (1967).

CHAPTER 3

Standard methods of describing heavy-ion processes.

Two methods are commonly used for describing the heavy-ion elastic scattering, inelastic excitations and transfer reactions. One is based on the semi-classical concepts, and the other one is a quantal method. We shall illustrate the semi-classical method on the example of elastic scattering, and the quantal method on the examples of one- and two-nucleon transfer reactions. In the latter the standard quantal method is known as the « distorted-wave Born approximation » (DWBA) formalism. It is also known an interesting approach which exposes the Fresnel type of diffractive scattering [3.16]. In this approach one gets closed expressions for both the elastic and the inelastic heavy-ion scattering, and the resulting formulae display the interference patterns observable in the angular distributions and excitation functions. For more details about this approach and its applicability we refer to the recent papers [3.16] based on this formalism with further references included there.

3.1. – The semi-classical method.

Let us consider elastic scattering, say, of the ^{16}O ions on ^{58}Ni. We take as given the central potential $V(r)$, describing the interaction of the two nuclei. For the Newtonian motion on an orbit in the field $V(r)$ we evaluate a quantity named the deflection function. It is

$$\theta(b) = \pi - 2\int_{r_0}^{\infty} \mathrm{d}r \frac{b}{r^2}\left[1 - \frac{b^2}{r^2} - \frac{V(r)}{E}\right]^{-\frac{1}{2}}, \tag{3.1}$$

where r_0 is the turning point, *i.e.* the classical distance of the closest approach, b is the impact parameter, related to the angular momentum l by $kb = l$, $E = k^2(2\mu)^{-1}$ and μ is the reduced mass, θ is the angle by which a classical particle with energy E and angular momentum l (thus also with a fixed impact parameter b) gets deflected in the central potential $V(r)$.

To get more acquainted with the deflection function, let us consider for the moment $V(r)$ as given by the pure Coulomb interaction. In fig. 3.1 we plot the deflection function, and note a unique correspondence between b and $\theta(b)$.

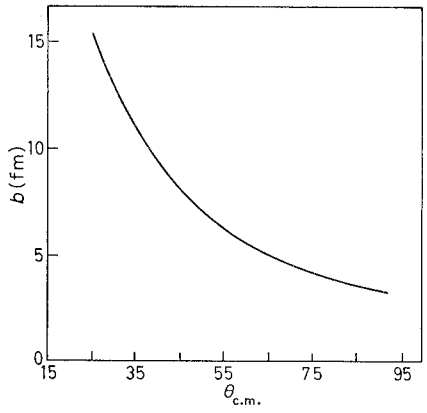

Fig. 3.1.

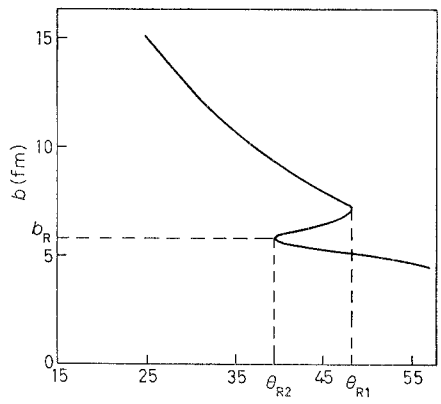

Fig. 3.2.

Fig. 3.1. – Deflection function $\theta(b)$ arising from a Coulomb potential—from ref. [3.1].

Fig. 3.2. – Deflection function $\theta(b)$ for the scattering of ^{16}O on ^{58}Ni at $E_{lab} = 60$ MeV—from ref. [3.1]. The real potential was taken in the Woods-Saxon form $V(r) = V_R[1 + \exp[(r - R)/a]]^{-1}$ with $V_R = -7$ MeV, $R = 9.65$ fm, $a = 0.6$ fm.

A different character has the deflection function for $V(r)$ being the Woods-Saxon potential. It is plotted in fig. 3.2 and we note that for some angles there are three values of impact parameter. All of them must be included. In fig. 3.2

other two points appear also around which the deflection function has parabolic shape. Scattering angles corresponding to these points are called *rainbow* scattering.

In the pure classical theory the differential cross-section can be obtained from the derivative of the inverse function of $\theta(b)$. We have

$$\left(\frac{\mathrm{d}\sigma}{\mathrm{d}\Omega}\right)_{\text{classical}} = \frac{b\,\mathrm{d}b}{\sin\theta\,\mathrm{d}\theta}\,. \tag{3.2}$$

The semi-classical method uses some concepts of the classical theory, but also incorporates some quantal features. KOELING and MALFLIET in ref. [3.17] indicated how the semi-classical approach can be derived from the Feynman path integral method. In the formalism the heavy-ion trajectories are extended to complex ones, by using an analytic continuation of the Hamilton equations. To get the prescription for the evaluation of $\mathrm{d}\sigma/\mathrm{d}\Omega$ in the semi-classical model we begin from the standard quantal formula for $\mathrm{d}\sigma/\mathrm{d}\Omega$. We write

$$\frac{\mathrm{d}\sigma}{\mathrm{d}\Omega} = |f(\theta)|^2\,, \qquad f(\theta) = \frac{i}{2k}\sum_{l=0}^{\infty}(2l+1)\left(1-\exp\left[2i\delta_l\right]\right)P_l(\cos\theta)\,. \tag{3.3}$$

In order to evaluate the phase shifts δ_l's we take advantage of the fact that for heavy-ion scattering the relatively large reduced masses give rise to large values of $k = \sqrt{2\mu E}$ even at moderate energies E. The large value of the wave number k justifies the use of an approximate treatment of the Schrödinger equation known as the WKB (Wentzel-Kramers-Brillouin) method.

The WKB approximation is discussed in many textbooks, see, *e.g.*, ref. [3.3]. We will only state the final result and discuss its physical background. The basic assumption is that, at large k, the main effect of the potential is to modulate the phase of the wave function, hence the radial solutions of the wave equation may be tried in the form

$$\mu_l(r) = \exp\left[\pm i\phi(r)\,k\right].$$

If we assume further that the distance d over which the potential $V(r)$ changes significantly is large compared with the wave-length $\lambda = k^{-1}$, *i.e.* $kd \gg l$, one can neglect $\mathrm{d}^2\phi/\mathrm{d}r^2$. The third assumption in the WKB method is the condition that the radial wave function vanishes at the so-called turning point r_0, determined through the relation

$$\frac{k^2}{2\mu} = V(r_0) + \frac{(l+\frac{1}{2})^2}{2\mu r_0^2}\,. \tag{3.4}$$

This boundary condition clearly has a motivation borrowed from classical mechanics, where a particle cannot penetrate past the point in which the kinetic

energy equals the effective-potential (real potential plus centrifugal energy) barrier.

The WKB method gives the following expression for the l-th partial scattering phase shift:

$$\delta_l^{\mathrm{WKB}}(k) = \tfrac{1}{2}\pi(l+\tfrac{1}{2}) - kr_0 + \int_{r_0}^{\infty}[k(r)-k]\,\mathrm{d}r, \tag{3.5}$$

where

$$k(r) = k[1-(l+\tfrac{1}{2})^2(kr)^{-2} - V(r)E^{-1}]^{\frac{1}{2}}$$

and the turning point r_0 is determined from $k(r_0) = 0$.

The WKB formalism may be extended to complex potentials such as the optical-model potential [3.3]. In this case r_0 becomes complex and the integral in (3.5) is in the complex plane from the complex turning point to real infinity.

A difficulty arises if there exist multiple solutions for r_0. A possible choice is to take then the solution with the largest real part and the smallest negative imaginary part corresponding to reflection at the first barrier. The ambiguity can be a source of error only for a very few partial waves which are tunnelling through the first potential barrier. At energies near the Coulomb barrier this occurs only for the lower partial waves, where the error is reduced by the absorptive part of the optical potential. For energies above the Coulomb barrier these ambiguities are less important and disappear completely at high energies.

Comparing eqs. (3.5) and (3.1) it is appropriate to notice the very close relationship between a derivative of the WKB phase shift and the classical deflection function. We have

$$2\frac{\mathrm{d}\delta_l^{\mathrm{WKB}}}{\mathrm{d}l} = \theta(l) \tag{3.6}$$

with the relation $kb = l + \frac{1}{2}$ kept in mind.

An example of the partial phase shifts is given in fig. 3.3 for the elastic scattering $^{18}O + {}^{120}Sn$ at 100 MeV [3.4]. One can see that only partial waves with $50 \leqslant l \leqslant 70$ are contributing to the scattering amplitude. The relatively small interval of large values of l is a typical feature for scattering of heavy ions.

The smallness of the interval of the effective l's is the result of strong absorption at the surface and of attractive force which sucks high-angular-momentum orbits into the absorbing region. The large values of l arise because of large radii of heavy ions and large values of k; roughly the half-value of $|\exp[2i\delta_l]|$ occurs at $l_0 = kR$, R being the radius of the potential.

The WKB method helps us in getting information about the phase shift, but to evaluate the cross-section we must know the amplitude $f(\theta)$, *i.e.* we must perform the summation in eq. (3.3). This may be simplified as follows. Because of strong absorption the sum over partial waves is determined mainly

by the terms with large l. Hence we can replace $P_l(\cos\theta)$ by the asymptotic expression for large l

$$P_l(\cos\theta) \approx \left[\frac{\pi}{2}\left(l+\frac{1}{2}\right)\sin\theta\right]^{-\frac{1}{2}} \sin\left[\left(l+\frac{1}{2}\right)\theta+\frac{\pi}{4}\right], \tag{3.7}$$

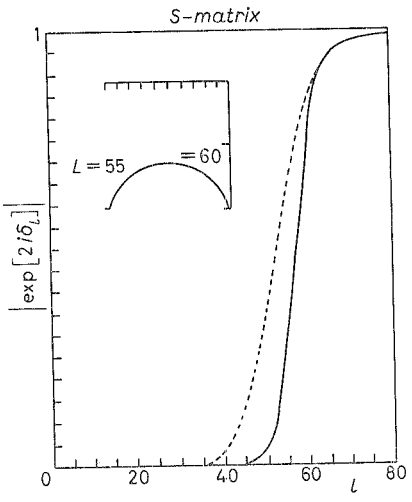

Fig. 3.3. – The amplitude of $\exp[2i\delta_l]$ for the elastic scattering $^{18}O+^{120}Sn$ at $E=100$ MeV (ref. [3.4]), corresponding to the Woods-Saxon potential $V(r)=(V_R+iV_I)\cdot[1+\exp[(r-R)/a]]^{-1}$ with parameters $V_R=-40$ MeV, $V_I=-15$ MeV, $a=0.45$ fm, $R=1.31$ fm $(A_1^{\frac{1}{3}}+A_2^{\frac{1}{3}})$. The dashed line corresponds to $V_R=0$ and shows by comparison how the real potential sucks high l's into the absorbing region.

omitting from considerations $\theta=0,\ \pi$.

Substituting this in (3.3) and replacing the sum by an integral (thus assuming that the phase shift is a smooth function of l), one obtains

$$f(\theta) \approx -(2\pi k\sin\theta)^{-\frac{1}{2}}\int_0^\infty dl\,(l+\tfrac{1}{2})^{\frac{1}{2}}(\exp[i\varphi_+]-\exp[i\varphi_-]), \tag{3.8}$$

where

$$\varphi_\pm = 2\delta_l \pm\left(l+\frac{1}{2}\right)\theta \pm\frac{\pi}{4}.$$

Finally we evaluate the integral in eq. (3.8) using the method of stationary phase. We get that the main contribution comes from such values of l, denoted by l_i, for which the phases $\varphi_\pm$ have extrema. This is so because near the extremum the exponents vary slowly, hence in this region the exponential factors will

not cancel. Thus we have the condition

$$\left(\frac{\mathrm{d}\varphi_{\pm}}{\mathrm{d}l}\right)_{l=l_i} = 0\,, \tag{3.9}$$

from which there follows (see eqs. (3.6) and (3.8)) the relation

$$\pm\theta = \theta(l_i)\,, \tag{3.10}$$

$\theta(l_i)$ being the classical deflection function.

Having stationary points we expand δ_l around them up to the second order and explicitly evaluate the integral over l. From each stationary value we get a contribution to the scattering amplitude

$$f(\theta) = \sum_i f_i(\theta)$$

with

$$\begin{cases} f_i(\theta) = -k^{-1}\left(l_i + \frac{1}{2}\right)^{\frac{1}{2}}\left[2\sin\theta\left|\frac{\mathrm{d}^2\delta_l}{\mathrm{d}l^2}\right|_{l=l_i}\right]^{-\frac{1}{2}}\exp\left[i\alpha(l_i)\right], \\ \alpha(l_i) = \left[2\delta_l - 2\left(l+\frac{1}{2}\right)\frac{\mathrm{d}\delta_l}{\mathrm{d}l} - \frac{\pi}{4}\left(2 - \frac{\mathrm{d}^2\delta_l}{\mathrm{d}l^2}\Big/\left|\frac{\mathrm{d}^2\delta_l}{\mathrm{d}l^2}\right| - \frac{\mathrm{d}\delta_l}{\mathrm{d}l}\Big/\left|\frac{\mathrm{d}\delta_l}{\mathrm{d}l}\right|\right)\right]_{l=l_i}. \end{cases} \tag{3.11}$$

The differential cross-section is obtained in the semi-classical method as

$$\left(\frac{\mathrm{d}\sigma}{\mathrm{d}\Omega}\right)_{\text{semi-classical}} = \left|\sum f_i(\theta)\right|^2. \tag{3.12}$$

Therefore, the interference effects which are absent in the classical expression are present in the semi-classical formula.

In fig. 3.4 there is a plot of the ratio

$$\left(\frac{\mathrm{d}\sigma}{\mathrm{d}\Omega}\right)_{\text{semi-classical}} \Big/ \left(\frac{\mathrm{d}\sigma}{\mathrm{d}\Omega}\right)_{\text{Ruth}}$$

as the continuous line and it is compared with a plot of the same ratio evaluated exactly (broken line). Here « exact » means that we solve numerically the Schrödinger equation and find out the phase shifts l. The agreement is very good.

The semi-classical method can be extended to inelastic scattering with excited final states of the target and to one- or more-nucleon transfer reactions. The agreement with the experimental data is quite good, however, in cases in which the final state differs from the initial one, more assumptions are needed to write down an expression for the cross-section. In such a situation

the classical trajectory corresponding to the relative motion of ions in the initial state is different from the trajectory in the final state, and some averaging procedure is needed. One must also deal with an imaginary part of the optical po-

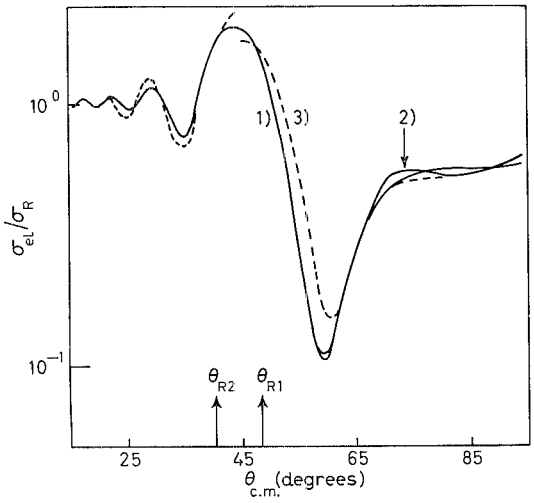

Fig. 3.4. – Elastic cross-section for scattering of ^{16}O on ^{58}Ni at $E_{lab} = 60$ MeV. The real-potential parameters are given in the caption of fig. 3.2. Curve 1) represents the exact calculations, curve 2) the semi-classical one, curve 3) the result obtained by the stationary-phase method.

tential, and evaluate reaction matrix elements from the set of 1st order differential equations, following from the time-dependent Schrödinger equation. This set of equations is solved numerically with the appropriate initial conditions. The whole procedure is rather involved, but the agreement with experimental data is very good. We end here our presentation of the semi-classical method and refer to BROGLIA *et al.* [3.5] and KOELING and MALFLIET [3.17] for more details.

3.2. – The quantal method.

The second standard method of treating heavy-ion processes is the quantal method. For elastic scattering it is known as the optical potential method and for inelastic scattering and transfer reactions as the distorted-wave Born approximation (DWBA), or the more accurate formalism known as the coupled-channel formalism.

3.2'1. *Optical model.* – In the elastic case one parametrizes real and imaginary parts of potential, most often assumed in the form of Woods-Saxon potential,

adds the Coulomb potential, solves numerically the Schrödinger equation and looks for the best parameters fitting the differential cross-section.

As an example we consider the scattering of the ^{16}O ions on ^{60}Ni at 60 MeV laboratory energy. The experimental data [3.7] are well fitted by the following total potential:

$$V(r) = V_N(r) + V_C(r) \tag{3.13}$$

with the nuclear part of the potential, V_N, a Woods-Saxon optical-model potential,

$$V_N(r) = \frac{V_R}{1 + \exp[(r - R_{0R})/a_{0R}]} + \frac{iW_I}{1 + \exp[(r - R_{0I})/a_{0I}]}, \tag{3.14}$$

and with a Coulomb potential V_C of the form

$$V_C(r) = \begin{cases} (Z_1 Z_2 e^2/2R_C)(3 - r^2/R_C^2), & r < R_C, \\ Z_1 Z_2 e^2/r, & r > R_C, \end{cases} \tag{3.15}$$

which is an extension to the case of heavy-ion scattering of the potential due to a point charge on a uniformly charged sphere. Presumably more correct for two heavy ions would be the potential of two uniformly charged spheres. However, because of nearly total absorption near the origin, where the difference in the various Coulomb potentials is largest, the scattering cross-sections are fairly insensitive to the choice of the model Coulomb potential.

The parameters appearing in eq. (3.14) and (3.15) were found to be

$$V_R = -25 \text{ MeV},$$
$$W_I = -15 \text{ MeV},$$
$$R_C = R_{0I} = R_{0R} = 1.3(A_1^{\frac{1}{3}} + A_2^{\frac{1}{3}}) \text{ fm} = 8.365 \text{ fm},$$
$$a_{0R} = a_{0I} = 0.5 \text{ fm}.$$

Figure 3.5 shows the fit; moreover, it gives a comparison of the « exact » calculation of the differential cross-section (made with ABACUS II) and the WKB method [3.6]. All results are displayed with respect to the Rutherford cross-section. As can be seen the agreement is quite good over the entire curve.

In general the WKB approximation agrees well with the optical-model cross-section for energies and angles of major interest, *i.e.* $E_{c.m.} > 40$ MeV, and angles over which $(d\sigma/d\Omega)_{Ruth}$ changes by three decades [3.6]. The WKB method fails for energies which are excessively low or angles which are excessively large. Thus in the example shown in fig. 3.5 beyond 100° the WKB curve shows diffraction peaks with maxima in $(d\sigma/d\Omega)_{Ruth} \approx 5 \cdot 10^{-4}$ and with a

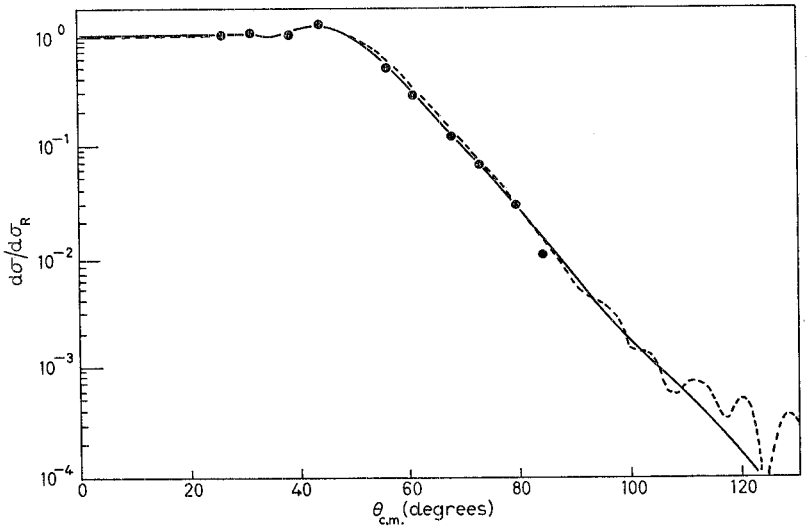

Fig. 3.5. – The reaction ^{60}Ni(^{16}O, ^{16}O)^{60}Ni at $E_{lab} = 60$ MeV—from ref. [3.6]: experimental points (•) taken from ref. [3.7] and calculations using ABACUS II (solid line) and WKB (dotted line).

much larger maximum at 180° $(d\sigma/d\Omega)_{Ruth} \approx 5 \cdot 10^{-3}$. On the contrary the exact calculation continues to decrease, levelling off at $(d\sigma/d\Omega)_{Ruth} \approx 8.2 \cdot 10^{-6}$ at 180°.

At high energies the WKB method, being fairly insensitive to values of k, may, however, be numerically superior than the exact procedure the effectiveness of which rapidly decreases for large k. For large k the numerical integration of the Schrödinger equation becomes a very difficult task because of the fine integration meshes required.

3.2'2. *The* DWBA *method.* – Let us now pass to transfer reactions and show some details of the evaluation of differential cross-section within the DWBA method [3, 8]. We denote by t the transferred subsystem and by c_1, c_2 the cores with which t is making up a bound state in the initial and final state,

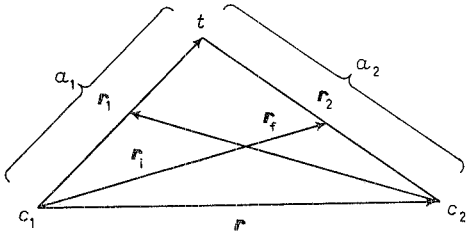

Fig. 3.6. – The vector diagram for the transfer reaction $(c_1, t) + c_2 \to c_1 + (c_2, t)$.

respectively. These bound systems we denote as $a_1 = (c_1, t)$ and $a_2 = (c_2, t)$ and our transfer reaction is

$$(c_1, t) + c_2 \to c_1 + (c_2, t) \qquad \text{or} \qquad a_1 + c_2 \to c_1 + a_2 . \tag{3.16}$$

The basic three bodies c_1, c_2 and t are depicted in fig. 3.6 at the vertices of a triangle, their relative distances are the sides of triangle, and $\boldsymbol{r}_i$, $\boldsymbol{r}_f$ denote the relative distance between the projectile and the target in the initial and in the final state, respectively.

In the DWBA method one assumes that

a) the interaction between projectile and target, before or after the tranfer took place, can be described in the initial and final state in terms of the optical potentials $U_{a_1c_2}$ and $U_{c_1a_2}$, respectively;

b) these optical potentials do not differ too much from the interaction between cores $V_{c_1c_2}$;

c) the matrix element for a transfer process is proportional to the residual interaction, which is sandwiched between the states which are products of bound-system wave functions of a_1 and a_2 and distorted waves in the initial and final states, respectively.

Then the differential cross-section for transfer process can be schematically written as

$$\frac{\mathrm{d}\sigma}{\mathrm{d}\Omega} \approx S_1 S_2 |\langle \chi_f^{(-)}(\boldsymbol{k}_f, \boldsymbol{r}_f)\phi_2 | V_r | \chi_i^{(+)}(\boldsymbol{k}_i, \boldsymbol{r}_i)\phi_1 \rangle|^2 , \tag{3.17}$$

where S_1, S_2 are the so-called spectroscopic factors, uniquely defined by the initial and final bound-state structures. They measure the strength of a given state of t in the bound systems a_1, a_2 respectively; χ_i, χ_f are distorted waves describing the relative motion of a_1 and c_2 or a_2 and c_1 interacting via $U_{a_1c_2}$ or $U_{a_2c_1}$, respectively; ϕ_1, ϕ_2 are the bound-state wave functions of t in a_1, a_2, respectively; V_r is the residual interaction, describing the interaction which is not included in distorted waves. It depends on a representation and in the post-representation it is

$$V_r = V_{c_1a_2} - U_{c_1a_2} = (V_{c_1t} + V_{c_1c_2}) - U_{c_1a_2} \approx V_{c_1t} . \tag{3.18}$$

Here, V_{AB} denotes an effective interaction between A and B and we have used $V_{c_1c_2} \approx U_{c_1a_2}$.

The matrix element in eq. (3.17) contains a 6-dimensional integral, very unpleasant to deal on a computer. To simplify the calculation especially below the Coulomb barrier, one usually makes some further approximations within the DWBA scheme:

a) Localization in the strong Coulomb field. Such a field favours large core-core distances, and therefore ϕ_2 can be reasonably approximated by its asymptotic form

$$\phi_2 \approx N_2 h_{l_2}^{(1)}(i\sqrt{2mB_2}r_2)\, Y_{l_2}\lambda_2(r_2)\,, \tag{3.19}$$

where N_2 is the normalization constant, B_2 is the binding energy of t in a_2, m the reduced mass in the (t, c_2) system, $h_l^{(1)}$ being the Hankel function.

b) No recoil, based on the smallness of the mass of transferred particle with respect to the mass of the bound system of this particle with the core. Looking at fig. 3.6, we write

$$\left\{\begin{aligned} &\chi_i^{(+)}(\boldsymbol{k}_i, \boldsymbol{r}_i) = \chi_i^{(+)}\left(\boldsymbol{k}_i, \boldsymbol{r} - \frac{m_t}{m_{a_1}}\boldsymbol{r}_1\right) \approx \chi_i^{(+)}(\boldsymbol{k}_i, \boldsymbol{r})\,, \\ &\chi_f^{(-)}(\boldsymbol{k}_f, \boldsymbol{r}_f) = \chi_f^{(-)}\left(\boldsymbol{k}_f, \left(1 - \frac{m_t}{m_{a_2}}r - \frac{m_t}{m_{a_2}}\boldsymbol{r}_1\right)\right) \approx \chi_f^{(-)}\left(k_f, \left(1 - \frac{m_t}{m_{a_2}}\right)\boldsymbol{r}\right) \approx \\ &\qquad\qquad \approx \chi_f^{(-)}\left(\left(1 - \frac{m_t}{m_{a_2}}\right)\boldsymbol{k}_f, \boldsymbol{r}\right). \end{aligned}\right. \tag{3.20}$$

The last step is true if the function χ_i depends only on the product of momentum and position variables, as in the case of pure Coulomb wave functions. The no-recoil approximation enables us to replace a 6-dimensional integral by a product of two 3-dimensional integrals.

Next one of the 3-dimensional integrals is replaced by a one-dimensional integral and a sum over angular momentum, by using a property of the Hankel function which was put in instead of ϕ_2. The final formula for the one-nucleon transfer differential cross-section [3.9] is

$$\frac{\mathrm{d}\sigma}{\mathrm{d}\Omega} = 4\pi \frac{m_i m_f}{(2\pi\hbar^2)^2}\frac{k_f}{k_i}\frac{2a_2+1}{(2c_2+1)(2j_2+1)} S_{j_1 l_1} S_{j_2 l_2} |A_{l_1}|^2 |N_2|^2 \cdot \cdot \sum_{l\lambda} \left\langle j_1 \frac{1}{2} l0 \,\middle|\, j_2 \frac{1}{2}\right\rangle |T_{l\lambda}(\theta)|^2\,, \tag{3.21}$$

where

m_i, m_f are reduced initial and final masses;

j_1, j_2 are total angular momenta of nucleon bound in a_1, a_2, respectively, and similarly l_1, l_2;

$$A_{l_1} = \int \mathrm{d}r_1\, r_1^2 j_{l_1}(i\sqrt{2mB_2\hbar^{-2}}r_1)\, V_{nc_1}(r_1)\mu_{l_1}(r_1)\,;$$

$$T_{l\lambda}(\theta) = \int \mathrm{d}^3 r\, \chi_f^{(-)*}\left(\left(1 - \frac{m}{m_{a_2}}\right)\boldsymbol{k}_f, \boldsymbol{r}\right) h_{l_2}^{(1)}(i\sqrt{2mB_2\hbar^{-2}}r)\, Y_{l\lambda}(r)\, \chi_i^{(+)}(\boldsymbol{k}_i, \boldsymbol{r})\,;$$

$\mu_{l_1}(r)$ is the radial wave function of the nucleon in the (n, c_1) bound state.

The values of l are bounded by the following conditions:

$$|l_1 - l_2| \leqslant l \leqslant l_1 + l_2 ,$$
$$|j_1 - j_2| \leqslant l \leqslant j_1 + j_2 ,$$
$$(-1)^{l_1+l_2} = (-1)^l .$$

This formalism was developed by BUTTLE and GOLDFARB [3.9] and was very successful in interpreting many experiments. For illustration we show in fig. 3.7 results obtained for the total cross-section with spectroscopic factors in agreement with the shell model predictions.

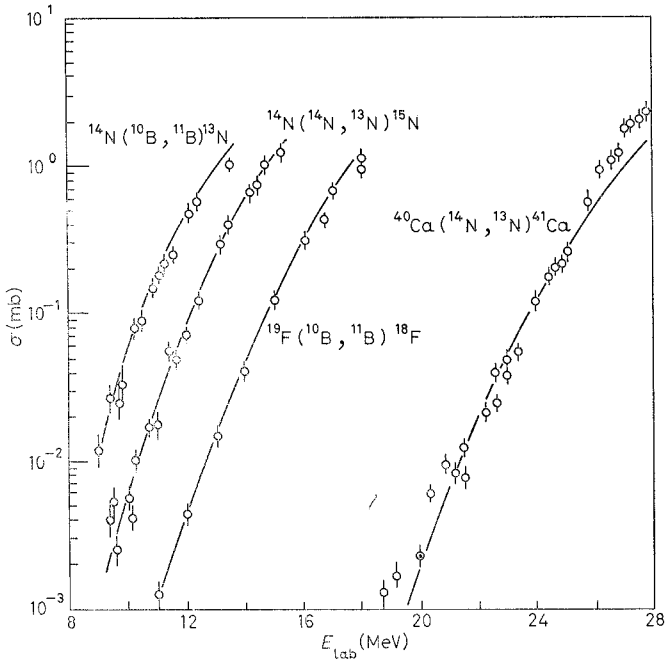

Fig. 3.7. – The total cross-section of the one-nucleon transfer reactions (from ref. [3.8]).

Another example of a very good fit of the DWBA, no-recoil, finite-range method, is given in fig. 3.8, for one-nucleon transfer processes at different laboratory energies.

There are three characteristic features to note:

i) the angular distributions have a bell shape,

ii) the bell becomes narrower for higher energies,

iii) the maximum of the bell is moving forward for higher energies.

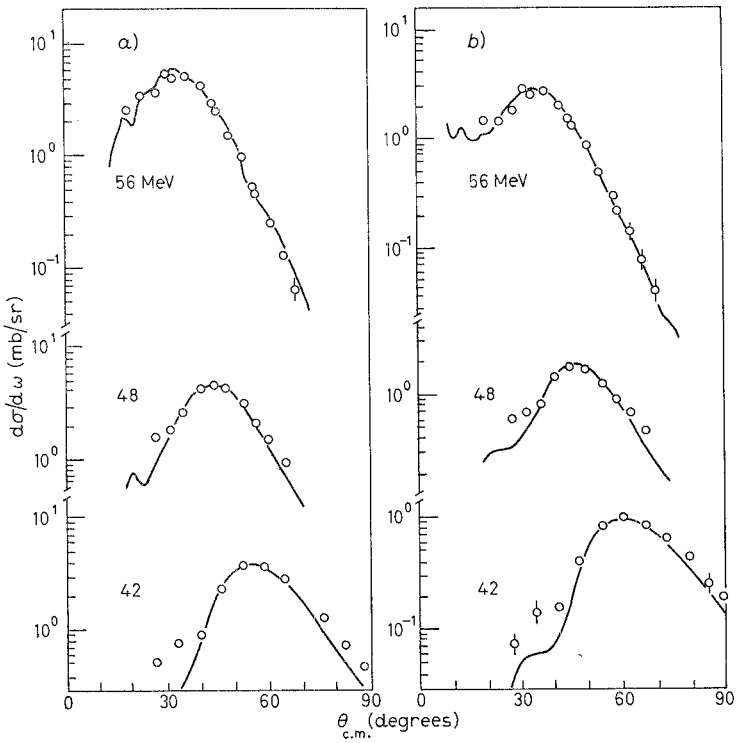

Fig. 3.8. – Angular distributions for the $^{48}Ca(^{16}O, ^{15}N)$ reaction to *a*) the $1f_{\frac{7}{2}}$ ground state and *b*) the $2p_{\frac{3}{2}}$ excited state in ^{49}Sc. The solid lines represent DWBA calculations performed with the no-recoil code (from ref. [3.10]). *a*) $E_X = 0$ MeV, $L = 4$; *b*) $E_X = 3.08$ MeV, $L = 2$.

The bell shape angular distributions are connected with the phenomenon of grazing collision. It arises because of the strong, repelling Coulomb force, on one side, and the strong nuclear absorption, on the other side. The most favourable scattering angle for nucleon transfer is called the *grazing angle*, and in terms of classical trajectories it corresponds to well-matched initial and final trajectories.

It should be pointed out that in order to get a good agreement of the DWBA fits with the experimental data it is often necessary to include extra normalization factors ranging up to 3.5.

3.3. – Difficulties of the standard methods.

In spite of good fits obtained by the semi-classical and DWBA methods there is a number of problems connected with these methods. We shall make a few remarks about the semi-classical method (for a more complete account

ot the semi-classical method see ref. [3.5, 3.17]) and concentrate our attention on the difficulties of the DWBA scheme.

For transfer reactions the semi-classical method finds difficulty in coping with different initial and final trajectories and some *ad hoc* averaging procedure is invoked to cure this disease. Troubles also arise in defining the phase in the semi-classical method. The WKB and stationary-phase methods come with some help in defining the semi-classical phase, but with different initial and final trajectories it is only a heuristic argument and, in fact, for the transfer reaction a definite phase must be assumed and cannot be derived. There are also some recipes about how to evaluate the cross-section for the transfer processes and the geometrical mean value seems to be accepted, though, including the arbitrariness in phase, they do not follow from any physical assumption. On the computational side, the difficulties are in coping with very many partial waves and in solving very many coupled sets of differential equations. It becomes an enormous task to carry out such calculations even on big computers, thus limitations or further approximations must be contemplated.

Troubles of the DWBA method are quite numerous. They can be overcome in the sub-Coulomb region, but they manifest themselves above the Coulomb barrier, for the intermediate and high energies. To start with let us remind that the DWBA amplitude is a first term of a divergent series, as shown by GREIDER and DODD [3.11], within the 3-body formulation of rearrangement processes. For some processes like knock-out reactions it is possible to reformulate the infinite series in such a way that its term will be the t-matrix instead of the residual interaction V_r, and in this case one speaks about the DWTW amplitude. Such an amplitude is a first term of an infinite series which is generated by a kernel free from disconnected diagrams, thus it has a chance to be a convergent series, though the estimate of the importance of the 2nd-order and higher-order terms contributions is a separate, unanswered question.

In practice within the DWBA method one makes several additional approximations and above the Coulomb barrier, where both the nuclear and Coulomb forces interfere, one allows oneself for some change of parameters so that a good fit to the experimental data is achieved. Large ambiguities arise from not univocally defined parameters of the optical potential. Elastic scattering of ions in both initial and final states is needed as a separate set of data, but it does not fix up univocally the optical-potential parameters. Even if these parameters are determined from a partial-wave analysis of the elastic scattering, they are changed in the DWBA numerical programs to get better fits to the transfer processes. For sub-Coulomb energies there is much less uncertainty than above the Coulomb barrier, because of the dominance of the known Coulombic wave functions.

Another source of discrepancies within the DWBA scheme is in the spectroscopic factors. They should be given by the nuclear-structure theories and

may be looked at as predictions of the DWBA method, if a good fit to the cross-section is found. In practice, there are sometimes found such predictions of the DWBA scheme that the spectroscopic factors for different states do not agree with the nuclear-structure predictions, even by a factor 2 and then one cures the situation by speaking about the ratio of spectroscopic factors. The inconsistency in spectroscopic factors can be noted also if one compares the

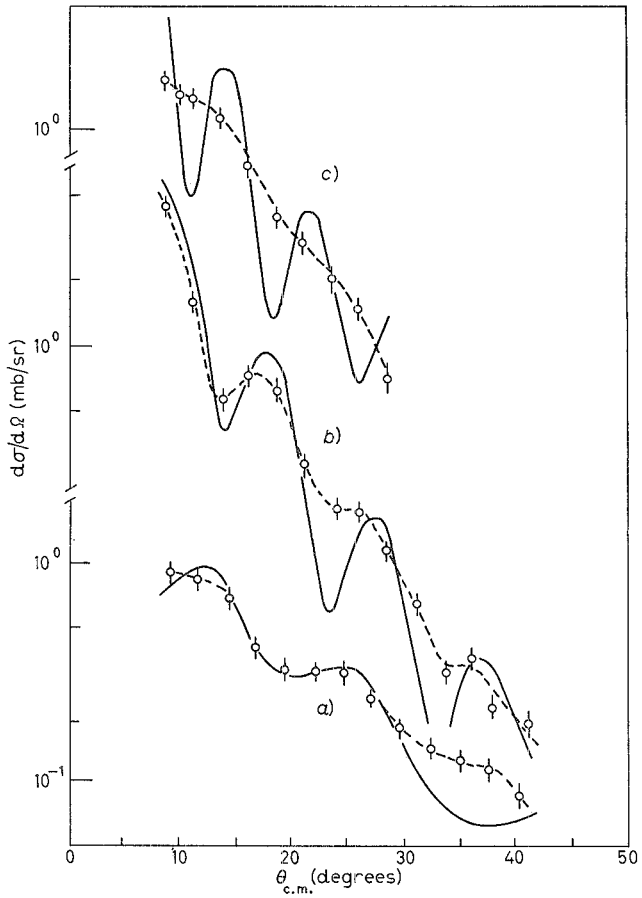

Fig. 3.9. – Differential cross-sections for the reaction $^{11}B(^{14}N, ^{15}O)^{10}Be$ at (curves *a*)) 41, (curves *b*)) 77 and (curves *c*)) 113 MeV compared with no-recoil DWBA calculations, which predict increasing diffraction structure at the highest energy, in contrast to the featureless experimental data—from ref. [3.12]. $Q = -3.96$ MeV, $l = 2$, — — — experimental, ——— DWBA.

same factors found in different reactions. These discrepancies have a tendency to increase with increasing energy. Only for sub-Coulombic processes there is a small discrepancy in determining spectroscopic factors by the DWBA scheme.

An important problem of the DWBA method is the question of recoil, especially for energies high enough above the Coulomb barrier. Below the Coulomb barrier the effect of recoil is small and may be safely neglected. However, let us look at the one-nucleon transfer reaction $^{11}B(^{14}N, ^{15}O)^{10}Be$ and watch

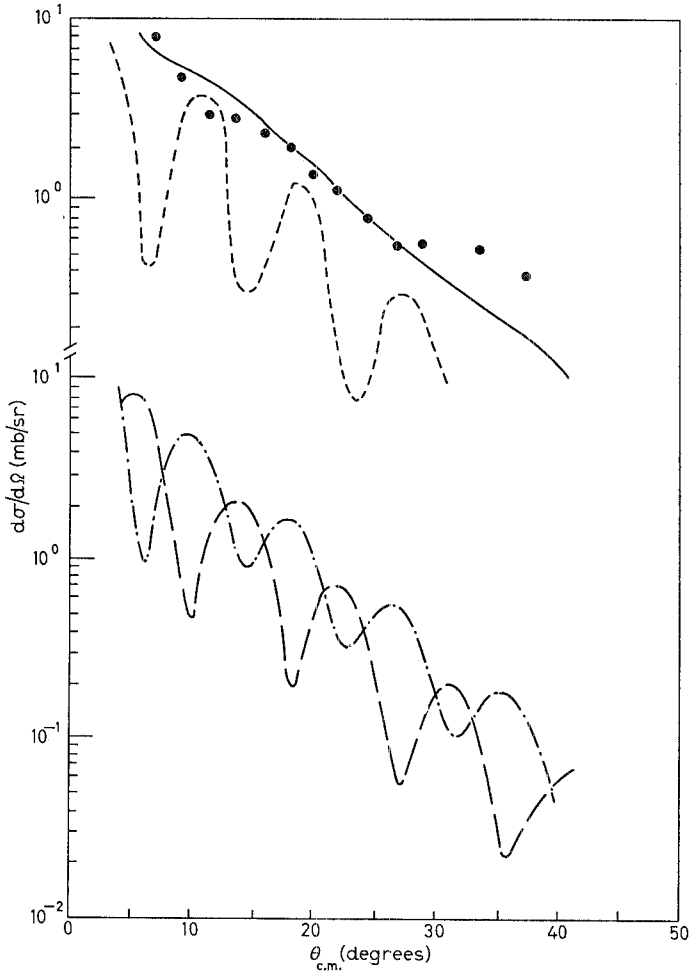

Fig. 3.10. – Theory (ref. [3.13]) and experiment (ref. [3.14]) for the $^{12}C(^{14}N, ^{13}C)^{13}N$ reaction. $E = 78$ MeV; • DWBA with recoil, $\sum l = 0.1$; ——— DWBA without recoil, $l = 0$ only; —·—·— $l = 0$; ——— $l = 1$.

the variation of the angular distribution with increasing energy. In fig. 3.9 the solid line gives the prediction of no-recoil DWBA amplitude, while the broken line goes through the experimental points to guide the eye. For the laboratory energy 113 MeV the DWBA no-recoil amplitude gives quite a wrong prediction.

DE VRIES [3, 13] among others analysed the influence of recoil and in fig. 3.10 we show his study of recoil in the reaction $^{12}C(^{14}N, ^{13}C)^{13}N$ at 78 MeV laboratory energy. The featureless shape of experimental angular distribution, contrary to the oscillatory character of the no-recoil DWBA amplitude, can be understood if two contributions, arising in the case of included recoil, are added together. The oscillatory dips are filled up by maxima of the other contribution. It is nice for the DWBA method that the inclusion of recoil puts it back into agreement with the data, but it forces us to use rather involved numerical programs, which can cope with 6-dimensional integrals.

The emphasis on recoil effects has also been made by DODD and GREIDER [3.15] in their analysis of recoil damping in heavy-ion transfer reactions. They found within the DWBA method that keeping the effect of finite mass of transferred particle resulted in the appearance of a recoil phase factor which gives strong damping of the diffraction oscillations. Due to this damping a featureless angular distribution appears which drops down as an inverse power of momentum transfer. Such behaviour is indeed suggested by the experimental data shown in fig. 3.11 lying very well on the line q^{-4}. As stated by DODD and GREIDER, in view of the simplification of their model and limitations of

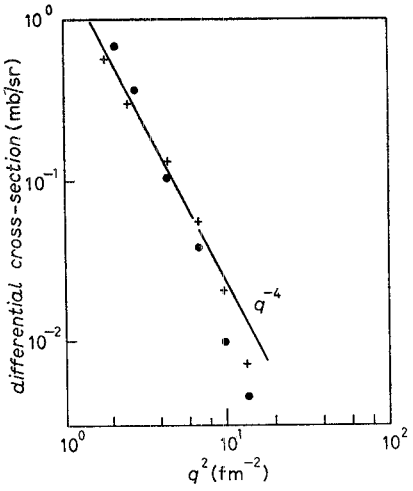

Fig. 3.11. – Differential cross-sections for the three-nucleon transfer reaction $^{12}C+^{12}C \rightarrow$ $\rightarrow {}^{9}Be+{}^{15}O$. The data fall uniformly on an exponentially decreasing curve predicted by DWBA calculations including recoil (from ref. [3.12]). $E_c = 114$ MeV, • $E_x =$ $= 15.08$ MeV, + $E_x = 12.87$ MeV.

DWBA, their result should not be taken as the whole explanation, but it suggests that at energies well above the Coulomb barrier recoil effects must be included.

Other plagues of DWBA method are the post-prior discrepancy and numerical problems in dealing with many partial waves with which highly oscillating functions are associated. The post-prior asymmetry is generated by approximations within the DWBA, in particular the neglect of recoil effects, but also by the inadequacy of treating in a consistent symmetrical way the initial and final channel when approximating the residual potential. We refer here, for example, to the approximation made in the previous section where the core-core interaction $V_{c_1c_2}$ was approximated by the optical potential corresponding to the final channel. The 6-dimensional integral codes, which enable us to take care of recoil, remove the post-prior discrepancy, providing we do not make an approximation about the residual interaction. The plague of very many partial waves in the relative motion of heavy ions becomes very severe at high energies. The impact parameter picture suggests itself as a more proper language than the partial-wave analysis.

REFERENCES

[3.1] R. A. MALFLIET: in *Estended Seminar on Nuclear Physics* (Trieste, 1973).
[3.2] N. F. MOTT and H. S. W. MASSEY: *The Theory of Atomic Collisions* (Oxford, 1965).
[3.3] P. C. SABATIER: *Nuovo Cimento*, **37**, 1180 (1965).
[3.4] N. K. GLENDENNING: *Rev. Mod. Phys.*, **47**, 659 (1975).
[3.5] R. A. BROGLIA, S. LANDOWNE, R. A. MALFLIET, V. ROSTOKIN and A. WINTHER: *Phys. Rep.*, **11** C, 1 (1974).
[3.6] T. W. DONNELLY, J. DUBACH and J. D. WALECKA: *Nucl. Phys.*, **232** A, 355 (1974).
[3.7] F. D. BECCHETTI, P. R. CHRISTENSEN, V. I. MANKO and R. Y. NICKELS: *Nucl. Phys.*, **203** A, 1 (1973).
[3.8] L. J. B. GOLDFARB: in *Oak Ridge Heavy-Ion Summer Study*, edited by S. T. THORNTON (Oak Ridge, Tenn., 1972).
[3.9] P. J. A. BUTTLE and L. J. B. GOLDFARB: *Nucl. Phys.*, **78**, 409 (1966); **176** A, 299 (1971).
[3.10] H. J. KÖRNER, G. C. MORRISON, L. R. GREENWOOD and R. H. SIEMSSEN: *Phys. Rev. C*, **7**, 107 (1973).
[3.11] R. L. DODD and K. R. GREIDER: *Phys. Rev.*, **146**, 671, 675 (1966).
[3.12] D. K. SCOTT: in *Symposium on Heavy-Ion Transfer Reactions* (Argonne, Ill., 1973), p. 97.
[3.13] R. M. DE VRIES: in *Symposium on Heavy-Ion Transfer Reactions* (Argonne, Ill., 1973), p. 189.
[3.14] W. VON OERTZEN, M. LIU, C. CAVERZASIO, J. C. JACMART, F. POUGHEAN, M. RIOU, J. C. ROYNETTE and C. STEPAN: *Nucl. Phys.*, **143** A, 34 (1970); **165** A, 118 (1971).
[3.15] L. R. DODD and K. R. GREIDER: *Phys. Rev.*, **180**, 1187 (1969).
[3.16] W. E. FRAHN and D. H. E. GROSS: *Ann. of Phys.*, **101**, 520 (1976); W. E. FRAHN: *Nucl. Phys.*, **272** A, 413 (1976); W. E. FRAHN and K. S. REHM: *Lett. Nuovo Cimento*, **17**, 339 (1976).
[3.17] T. KOELING and R. A. MALFLIET: *Phys. Lett.*, 22 C, 182 (1975).

CHAPTER 4

Methods based on the eikonal technique. Elastic scattering.

The eikonal technique, most popularly known in its special form as the Glauber model [4.1], has been commonly applied in the high-energy region for scattering of either elementary particles or a nucleus on another nucleus. Particular attention of this technique to heavy-ion processes has been brought in 1971 by DAR and KIRZON [4.2]. We shall come later to some details of this application, but now, staying within a more general view on the eikonal technique, not only restricted to the Glauber model, we mention several reasons which motivate the application of the eikonal approximation in studying the heavy-ion processes. They are the following:

a) The impact parameter representation, which is the language of the eikonal scheme instead of the partial-wave notion, is especially appropriate if one deals with very many partial waves arising either from the strong Coulomb field or increasing energy, or both.

b) The eikonal method is closely connected with the WKB method which in turn relates to the semi-classical method describing gross features of heavy-ion processes.

c) Below the Coulomb barrier, where the Coulomb interaction plays a dominant role, one can formulate the eikonal approximation in such a way that it gives the exact result for an arbitrary scattering angle and at all energies. Therefore, the association one usually has with the eikonal technique as appropriate for small scattering angle is removed in the case of dominating Coulomb field. At the Coulomb barrier and above, one must include also the strong nuclear force and for heavy ions one can again extend the eikonal technique to an arbitrary scattering angle. The large parameter is the ratio $D\lambda^{-1}$ mentioned in the introduction. We shall come back to this extension later in this chapter.

d) The eikonal technique, although an approximation, provides us often with an analytic, or almost analytic result, which can be studied from many points of view, contrary to outputs of numerical programs like that of the DWBA method, or semi-classical numerical codes.

e) It is much easier than in the standard methods to incorporate the 3-body and in general many-body aspects of scattering of composite systems if the propagation is simplified as in the eikonal method.

f) Some, even crude, trials of applying eikonal-type methods proved to be surprisingly successful. One may hope that more delicate use of the eikonal

technique will not destroy the agreement and will shed some light on the dynamics of heavy-ion processes at different energies.

We shall now review several ways of applying the eikonal method to heavy-ion processes and for clarity we divide our review into two big parts: one dealing with the elastic scattering (this chapter), another one with inelastic processes (chapter 5), and within these parts we consider separately different approaches.

4.1. – Glauber approximation.

The eikonal approximation may be derived straightforwardly, from the Schrödinger equation:

$$(\nabla^2 + k^2)\,\psi = 2\mu V(r)\,\psi\,, \tag{4.1}$$

μ being the reduced mass.

Thus, if one looks for a solution of the wave equation in the form

$$\psi = \phi(\boldsymbol{r}) \exp\left[i\boldsymbol{k}\cdot\boldsymbol{r}\right], \tag{4.2}$$

where ϕ is a slowly varying function over the range scaled with the wavelength $\lambda\!\!\!^{-} = k^{-1}$ (hence $\nabla^2\phi = 0$), one obtains from (4.1)

$$\frac{\partial\phi}{\partial z} = -i\frac{\mu}{k}\,V\phi\,, \qquad \phi(-\infty) = 1\,, \tag{4.3}$$

where the z-axis is chosen along the incidence direction $\boldsymbol{k}$.

The solution of eq. (4.3) is

$$\psi = \exp\left[ikz\right] \exp\left[-\frac{i}{v}\int_{-\infty}^{z} V(\boldsymbol{b}, \zeta)\,\mathrm{d}\zeta\right], \tag{4.4}$$

v being the relative velocity of colliding particles.

Putting this approximate wave function in the definition of the scattering amplitude, one has

$$f(\boldsymbol{q}) = -\frac{\mu}{2\pi}\int \mathrm{d}^2b \exp\left[i\boldsymbol{q}_\perp\cdot\boldsymbol{b}\right]\int \mathrm{d}z \exp\left[iq_\parallel z\right] V(b, z) \exp\left[-\frac{i}{v}\int_{-\infty}^{z} V\,\mathrm{d}\zeta\right], \tag{4.5}$$

$q_\perp$, $q_\parallel$ being the transverse and longitudinal momentum transfers, respectively.

The fact that for small-angle scattering at large momentum k one has

$$q_\perp \simeq q\,, \qquad q_\parallel \simeq 0 \tag{4.6}$$

allows us to perform the integration over the longitudinal co-ordinate z. Thus one arrives at the eikonal approximation in the form given by GLAUBER [4.1]:

$$f(q) = \frac{ik}{2\pi}\int \mathrm{d}^2b \, \exp\left[i\boldsymbol{q}\cdot\boldsymbol{b}\right]\Gamma(b) \,, \tag{4.7}$$

where

$$\Gamma(b) = 1 - \exp\left[i\chi(b)\right] \tag{4.8}$$

is called the profile function and the function $\chi(b)$ is given by the integral either along the direction of the incident beam or along the direction corresponding to the mean value of the initial and final momenta over the projectile-target interaction $V(r)$:

$$\chi(b) = -\frac{i}{v}\int_{-\infty}^{+\infty} \mathrm{d}z \; V(\sqrt{b^2 + z^2}) \,. \tag{4.9}$$

The function $\chi(b)$, called the eikonal (or Glauber) phase, is related to the phase shifts δ_l in the partial-wave expansion (3.3). In fact, for large k many partial waves are contributing to the scattering and one may put in (3.3)

$$\frac{i}{2k}\sum_l (2l+1) \to ik\int \mathrm{d}b \, b = \frac{ik}{2\pi}\int \mathrm{d}^2b \,, \tag{4.10}$$

where the relation $kb = l + \frac{1}{2}$ was used.

Further for $l \gg 1$ and small scattering angles ($\theta \ll 1$), one may put

$$P_l(\cos\theta) = J_0\big((l+\tfrac{1}{2})\theta\big) = J_0(qb) \,, \tag{4.11}$$

where $q = 2k\sin(\theta/2)$ is the c.m. momentum transfer.

Thus the partial-wave expansion (3.3), at large k and small θ, may be written exactly in the form of eq. (4.7) with

$$\chi(b) = 2\delta_l(k, l = kb) \,. \tag{4.12}$$

The equivalence of the Legendre sum (eq. (3.3)) and the Fourier-Bessel integral (eq. (4.7)) representations (in fact, there is a remarkable cancellation of the remainder functions from the two approximations (4.10) and (4.11)) allows us to write the eikonal approximation also in the form of the partial-wave expansion with the phase shifts equal to half of the Glauber phase (4.9).

The main advantage of the Glauber approximation (4.7)-(4.9) consists in its simplicity. Of extreme importance is that the interaction appears linearly

in the eikonal phase. In the case of scattering from a composite target, this leads to additivity of phase shifts from individual constituents which is a basic assumption of the Glauber model of multiple scattering (see **4.3**).

The framework of the Glauber approximation allows for a direct construction of the interaction from the phase shifts. In fact, the Glauber phase shift (eqs. (4.12) and (4.9)) may be written for spherical potential in the form

$$\delta^{\mathrm{Gl}}(b) = -\frac{1}{v}\int_b^\infty \frac{\mathrm{d}r\, r V(r)}{\sqrt{r^2 - b^2}}, \tag{4.13}$$

which is the integral equation for $V(r)$ of the Abel type. Its solution is

$$\frac{V(r)}{v} = \frac{2}{\pi}\frac{1}{r}\frac{\mathrm{d}}{\mathrm{d}r}\int_r^\infty \frac{\mathrm{d}b\, b\delta^{\mathrm{Gl}}(b)}{\sqrt{b^2 - r^2}}. \tag{4.14}$$

4.2. – Corrections to the Glauber approximation from WKB.

It is instructive to study the relation between the Glauber approximation and the WKB method [4.3, 4.4].

Equation (3.5) for the WKB phase shift may be written as follows:

$$\delta^{\mathrm{WKB}}(k, b) = k\int_{r_0}^\infty \frac{\mathrm{d}r}{r}\left[r^2\left(1 - \frac{V(r)}{E}\right) - b^2\right]^{\frac{1}{2}} - k\int_b^\infty \frac{\mathrm{d}r}{r}(r^2 - b^2)^{\frac{1}{2}}, \tag{4.15}$$

where $kb = l + \frac{1}{2}$.

Let us assume that the potential may be continued to the complex plane:

$$r \to \varrho = r + i\,\mathrm{Im}\,\varrho. \tag{4.16}$$

In order to proceed, it is convenient to introduce the following change of variable (Sabatier transformation [4.5]):

$$t(\varrho) = \varrho\left(1 - \frac{V(\varrho)}{E}\right)^{\frac{1}{2}}, \tag{4.17}$$

the inverse transformation being denoted by $\varrho = \varrho(t)$.

With this notation eq. (4.15) may be transformed to the form [4.4]

$$\delta^{\mathrm{WKB}}(k, b) = -\frac{1}{v}\int_b^\infty \frac{\mathrm{d}t\, t U(t)}{\sqrt{t^2 - b^2}} = -\frac{1}{v}\int_0^\infty \mathrm{d}z\, U\left(\sqrt{b^2 + z^2}\right), \tag{4.18}$$

where $U(t)$, called the quasi-potential, is defined as follows:

$$U(t) = vk \ln \frac{\varrho(t)}{t} . \tag{4.19}$$

Thus the WKB phase shift assumes the simple appearance of the Glauber phase shift (4.13), the essential difference being the replacement of the exact potential by a quasi-potential.

The relation between the potential and the quasi-potential may be written in the following compact forms:

$$U(t) = -E \ln \left[1 - \frac{V(\varrho)}{E}\right],$$

or

$$V(\varrho) = E\left[1 - \exp\left[-\frac{U(t)}{E}\right]\right], \tag{4.20}$$

where

$$\varrho(t) = t \exp\left[\frac{U(t)}{2E}\right], \qquad E = \frac{k^2}{2\mu} .$$

The Glauber approximation may be considered as the high-energy limit of the WKB method. If $V/E \ll 1$, the quasi-potential is simply the potential and the WKB and Glauber phase shifts coincide.

Expanding eq. (4.18) in a Taylor series about $1/k^2 = 0$, one obtains with the aid of eq. (4.20) [4.3]

$$\delta^{\mathrm{WKB}}(k, b) = \delta^{\mathrm{Gl}} + \delta^{(1)} + \delta^{(2)} + \dots ,$$

where

$$\begin{cases} \delta^{\mathrm{Gl}} = -\dfrac{1}{v}\displaystyle\int_0^\infty \mathrm{d}z\, V(\sqrt{b^2 + z^2}) , \\ \\ \delta^{(1)} = -\dfrac{1}{v^2 k}\displaystyle\int_0^\infty \mathrm{d}z\, \frac{\mathrm{d}}{\mathrm{d}r^2}[r^2 V^2(r)] , \\ \\ \delta^{(2)} = -\dfrac{2}{3v^3 k^2}\displaystyle\int_0^\infty \mathrm{d}z \left(\frac{\mathrm{d}}{\mathrm{d}r^2}\right)^2 [r^4 V^3(r)] . \end{cases} \tag{4.21}$$

It should be observed that the corrections to the simple Glauber result, because of the derivatives of the potential, are most important at the nuclear surface.

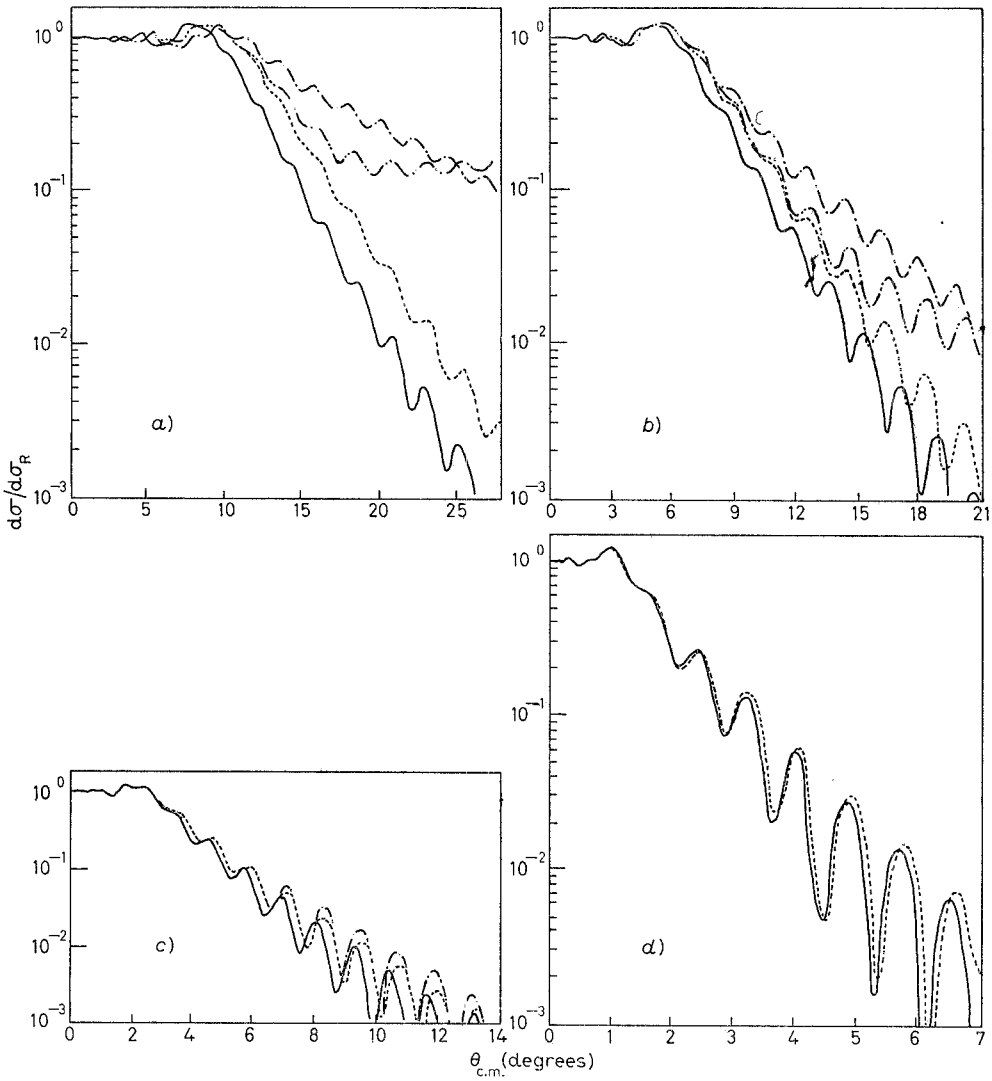

Fig. 4.1. – Elastic scattering ^{16}O-^{60}Ni at various c.m. energies as indicated. ··· WKB, ——— Glauber, —·—·— Glauber plus one-order correction, —··—··— Glauber plus two-order correction (from ref. [4.7]). In all cases the same optical-model parameters as for fig. 3.5 are used, although the « point-sphere » Coulomb potential in eq. (3.15) is replaced by the « sphere-sphere » Coulomb potential. *a*) 150 MeV, *b*) 225 MeV, *c*) 500 MeV, *d*) 1 GeV.

The relation of the Glauber approximation to the WKB method is illustrated in fig. 4.1 on the example of the elastic scattering ^{16}O-^{60}Ni for a series of c.m. energies [4.3].

Here the Glauber and WKB phase shifts are used in the partial-wave expansion (3.3). The full WKB result may be considered as a point of reference since, as explained in fig. 3.5, it should coincide with the exact optical-model calculation. In general, the Glauber approximation reproduces the qualitative shape of the curve quite well although it is shifted toward smaller angles and smaller cross-sections. With increasing energy the agreement between the Glauber and WKB results becomes more and more satisfactory. The WKB corrections greatly improve the positions of the maxima and minima in the curve, but the magnitude of the cross-section, although in excellent agreement at small angles, can be in serious error at large angles.

If the phase shifts are known eq. (4.18) may be viewed as an Abel integral equation and solved for the quasi-potential $U(t)$—compare eq. (4.14). Then the potential $V(r)$ can be constructed proceeding as follows [4.4]: Given $U(t)$, one can determine from (4.20) $V(\varrho)$ and ϱ for any value of the complex variable $t = t_R + it_I$. The true potential $V(r)$ is to be computed along the path in the complex t-plane given by Re $\varrho = r$, Im $\varrho = 0$. This condition provides, together with eq. (4.20), unequivocal relations $t_I = t_I(t_R)$, $r = r(t_R)$, and allows us to compute $V(r)$.

The potential constructed in such a way is an approximate solution to the inverse-scattering problem within the framework of the WKB approximation. It consequently has a wider range of validity than the Glauber approximation (eq. (4.14)) to which it reduces in the high-energy limit. The relation between the WKB and Glauber potentials has been studied by KUJAWSKI [4.4]. He assumed a specific and realistic form of the phase shifts and treated the resulting cross-sections, given by eq. (3.3), as « data ». The equivalent optical potential was constructed following the procedure described above—the WKB and Glauber potentials for α-^{42}Ca at 42 and 166 MeV are shown in fig. 4.2.

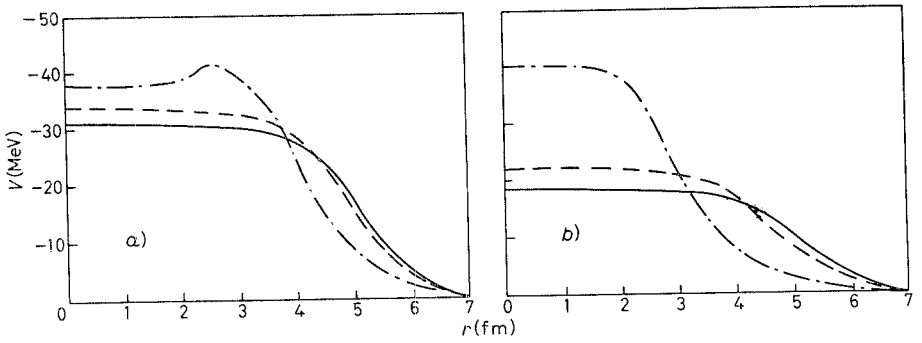

Fig. 4.2. – The real and imaginary parts of the calculated WKB [4.4] (dash-dotted line for α-^{42}Ca at 42 MeV, dashed line for α-^{42}Ca at 166 MeV) and Glauber (solid line) optical potentials. The nuclear phase-shift function was assumed in the form $\delta(b) = -((U_R + iU_I)/v)\int_0^\infty dz\,[1 + \exp[(r-R)/a]]^{-1}$. *a*) real part, *b*) imaginary part.

The validity of these potentials was then investigated by exactly solving the Schrödinger equation and comparing the resulting angular distributions with the corresponding « data »—see fig. 4.3. We see that the potentials obtained

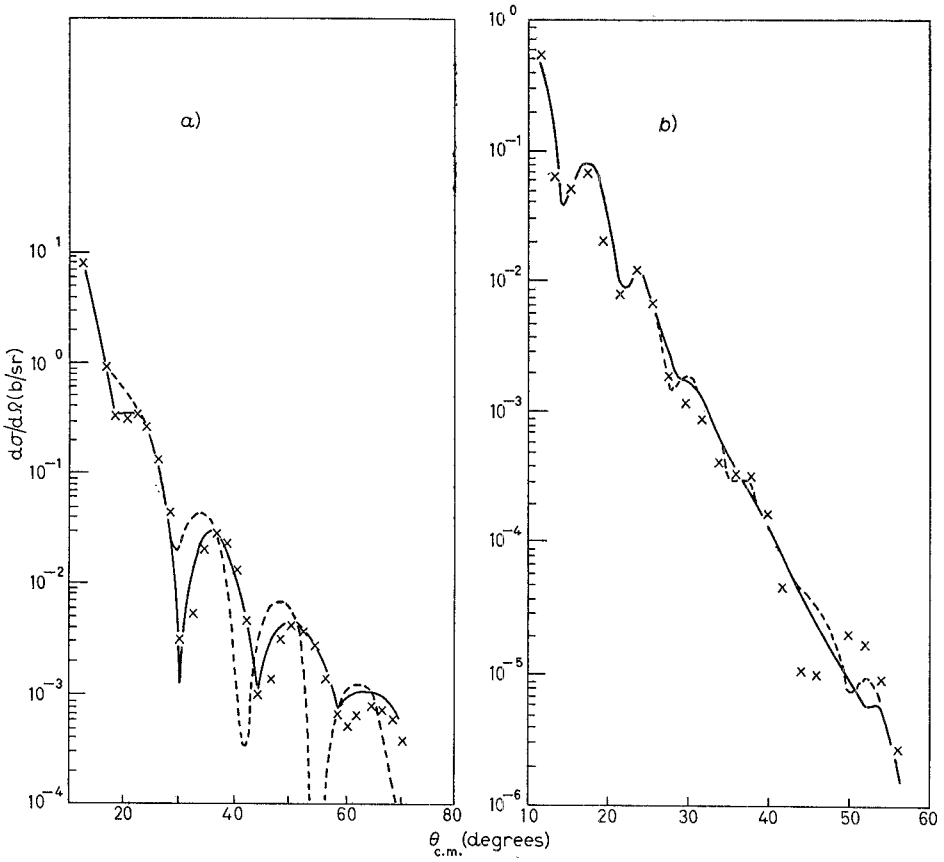

Fig. 4.3. – The elastic differential cross-section for the scattering of *a*) 42 MeV and *b*) 166 MeV α-particles by ^{42}Ca (ref. [4.4]). Solid line: solution for the WKB potential; dashed line: solution for the Glauber potential. The « data » points are denoted by crosses.

in the WKB approximation yield results in good agreement with the « data » up to 40°÷50°. The range of validity of the Glauber approximation is more limited. At larger angles both the approximations become unreliable.

4.3. – Glauber model of multiple scattering.

Let us consider the collision of two nuclei with A and B nucleons, respectively—see fig. 4.4.

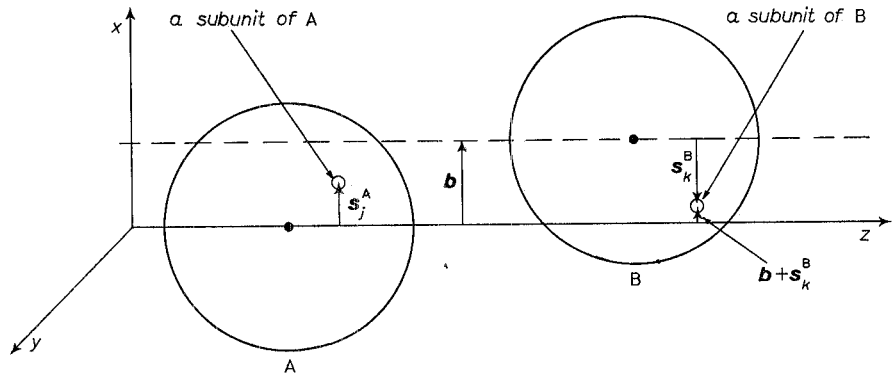

Fig. 4.4. – The geometry of collision A + B.

We assume that the total interaction between the incident and target nuclei is a sum of individual nucleon-nucleon (one from A, the other from B) interactions. Let us calculate now the phase shift for scattering of the two nuclei in the framework of the Glauber approximation—eq. (4.9). The fact that the interaction appears linearly in the Glauber phase leads to simple additivity of the individual nucleon-nucleon phase shifts:

$$\chi(b) = \sum_{j=1}^{A} \sum_{k=1}^{B} \chi_{jk}(\boldsymbol{b} - \boldsymbol{s}_j^A + \boldsymbol{s}_k^B) . \tag{4.22}$$

The additivity of phase shifts leads in turn to the following composition law for the profile function (4.8):

$$\Gamma(b) = 1 - \prod_{j=1}^{A} \prod_{k=1}^{B} \exp\left[i\chi_{jk}(\boldsymbol{b} - \boldsymbol{s}_j^A + \boldsymbol{s}_k^B)\right] = 1 - \prod_{j=1}^{A} \prod_{k=1}^{B} \left[1 - \gamma_{jk}(\boldsymbol{b} - \boldsymbol{s}_j^A + \boldsymbol{s}_k^B)\right], \tag{4.23}$$

where we have introduced the profiles for nucleon-nucleon collisions through a definition analogous to eq. (4.8). The elementary profiles $\gamma_{jk}(\boldsymbol{b} - \boldsymbol{s}_j^A + \boldsymbol{s}_k^B)$ may be expressed, by inverting the Fourier-Bessel transformation, through the nucleon-nucleon elastic-scattering amplitudes $f_{jk}(q)$, which are to be taken from the experiment with free particles.

In writing the above expressions we keep the projectile and target nucleons in the space positions given by the vectors $\boldsymbol{s}_j^A$, $\boldsymbol{s}_k^B$, respectively, in the plane of impact parameters, *i.e.* the plane perpendicular to the incident beam—see fig. 4.4. Hence we treat the nucleons as if they were frozen in a certain geometrical configuration. This assumption is justified if the time of collision is very short so that the projectile is gone before any rearrangement it induces in the target

can take place. Obviously one should then average over all possible internal configurations by sandwiching the operator of transition between the initial and final nuclear states.

Thus the final expression for the amplitude of transition in the Glauber model may be written as follows:

$$(4.24) \qquad F_{fi}(q) = \frac{ik}{2\pi}\int \mathrm{d}^2b \exp\left[i\boldsymbol{q}\cdot\boldsymbol{b}\right]\langle f_A f_B|\,1-\prod_{j=1}^{A}\prod_{k=1}^{B}\left[1-\gamma_{jk}(\boldsymbol{b}-\boldsymbol{s}_j^A+\boldsymbol{s}_k^B)\right]|i_A i_B\rangle\,,$$

i_A, i_B, f_A, f_B being the initial and final wave functions of the two nuclei. Equation (4.24) describes elastic as well as inelastic scattering. The inelasticity is meant here in nuclear sense, *i.e.* the nuclei may become excited or even broken up, but their constituents do not change in any essential way.

To summarize let us stress the main points underlying the Glauber model [4.1]:

a) high-energy small-angle scattering (eikonal approximation),

b) additivity of phase shifts,

c) expression of individual phase shifts (profiles) by means of elementary phenomenological elastic amplitudes,

d) averaging of the operator of scattering over the nuclear states.

If we multiply out the AB factors in the expression (4.23) we obtain the sum of terms with different powers of elementary profiles. This sum is finite (extending up to the AB-th order) and has alternating signs. The individual terms of this series are referred to as the contributions from single, double, triple, etc. scattering.

The different orders of scattering interfere with each other in a destructive way. The most important results of this interference are the diffractive structure (maxima and minima) of elastic angular distributions and the defect effect in the total cross-section.

Let us discuss in more detail the elastic scattering of heavy ions. We choose the matter densities of nuclei A, B in the form of independent-particle model (IPM):

$$(4.25) \qquad |i_A|^2 = |f_A|^2 = \prod_{j=1}^{A}\varrho_A(r_j^A)\,, \qquad |i_B|^2 = |f_B|^2 = \prod_{k=1}^{B}\varrho_B(r_k^B)\,.$$

It was shown by CZYŻ and MAXIMON [4.6] that for large A and B the expectation value of the profile operator (4.23) may be written then in the form

$$(4.26) \qquad \langle i_A i_B|\Gamma(b;\boldsymbol{s}_j^A,\boldsymbol{s}_k^B)|i_A i_B\rangle = 1-(1-\langle\gamma_{AB}\rangle)^{AB}\,,$$

where

$$(4.27)\qquad \begin{cases} \langle \gamma_{AB} \rangle = \int \mathrm{d}^2 s_A \, \mathrm{d}^2 s_B \, \varrho_A^{(2)}(s_A) \, \gamma(\boldsymbol{b} - \boldsymbol{s}_A + \boldsymbol{s}_B) \, \gamma_B^{(2)}(s_B) , \\ \varrho_A^{(2)}(s_A) = \int \mathrm{d}z \, \varrho_A(\boldsymbol{s}_A, z) , \\ \varrho_B^{(2)}(s_B) = \int \mathrm{d}z \, \varrho_B(\boldsymbol{s}_B, z) . \end{cases}$$

Thus for heavy-ion elastic scattering the Glauber model gives in the framework of IPM (eq. (4.25)) the following expression:

$$(4.28)\qquad F(q) = \frac{ik}{2\pi} \int \mathrm{d}^2 b \, \exp[i\boldsymbol{q}\cdot\boldsymbol{b}] \cdot$$

$$\cdot [1 - (1 - \langle \gamma_{AB} \rangle)^{AB}] \simeq \frac{ik}{2\pi} \int \mathrm{d}^2 b \, \exp[i\boldsymbol{q}\cdot\boldsymbol{b}] [1 - \exp[-AB \langle \gamma_{AB} \rangle]] ,$$

where in the second equation an exponentiation, justified for large A and B, has been carried out.

Since the amplitude assumes the simple appearance of the Glauber approximation for scattering in a potential field, the limit of large A and B is usually called the optical limit. The optical limit of the Glauber model provides a bridge between the phenomenological approach of the optical model and the microscopic description of multiple scattering. In fact, the optical phase shift and the equivalent optical potential can be expressed in terms of the microscopic quantities: nuclear densities and profiles of the elementary interaction. From eqs. (4.8), (4.9) and (4.28) one has

$$(4.29)\qquad \begin{cases} i\chi(b) = -AB \langle \gamma_{AB} \rangle , \\ V(b, z) = -ivAB \int \mathrm{d}^2 s_A \int \mathrm{d}^3 r_B \, \varrho_A(r_A) \, \gamma(\boldsymbol{b} - \boldsymbol{s}_A + \boldsymbol{s}_B) \, \varrho_B(r_B) . \end{cases}$$

These expressions may be simplified by noting that the elementary profile (being of size of the nucleon) is a very sharply peaked function compared to nuclear density. Thus to a good approximation one may put

$$(4.30)\qquad \gamma(\boldsymbol{b} - \boldsymbol{s}) = \frac{\sigma^{NN}(1 - i\alpha)}{2} \delta^{(2)}(\boldsymbol{b} - \boldsymbol{s}) ,$$

where the coefficient has been established from the optical theorem, σ^{NN} being the total nucleon-nucleon cross-section and α the ratio of the real to imaginary part for the forward elementary amplitude.

From eqs. (4.29) and (4.30) one obtains

$$(4.31)\qquad \begin{cases} i\chi(b) = -\dfrac{\sigma^{\mathcal{N}\mathcal{N}}(1-i\alpha)}{2} AB\int \mathrm{d}^2 s_{\mathrm{B}}\, \varrho_{\mathrm{A}}^{(2)}(\boldsymbol{b}-\boldsymbol{s}_{\mathrm{B}})\, \varrho_{\mathrm{B}}^{(2)}(s_{\mathrm{B}})\,, \\ V(r) = -iv\dfrac{\sigma^{\mathcal{N}\mathcal{N}}(1-i\alpha)}{2} AB\int \mathrm{d}^3 r_{\mathrm{B}}\, \varrho_{\mathrm{A}}(\boldsymbol{r}-\boldsymbol{r}_{\mathrm{B}})\, \varrho_{\mathrm{B}}(r_{\mathrm{B}})\,. \end{cases}$$

Thus the equivalent optical potential is proportional to the convolution of densities of the colliding nuclei.

The Glauber model has been extensively applied to the heavy-ion elastic scattering by DAR and KIRZON [4.2]. They write the scattering amplitude in the form of the partial-wave expansion. The phase shifts contain the Coulomb part, corresponding to the interaction between two point charges, and the nuclear part which is put equal to half (see eq. (4.12)) of the Glauber phase $\chi(b)$, as given in eq. (4.31). The explicit expression for the scattering amplitude $f(\theta)$ used by DAR and KIRZON is

$$f(\theta) = f_c(0) + \frac{1}{2ik}\sum_{l=0}^{\infty}(2l+1)\exp[2i\delta_l^c]\left(\exp[2i\delta_l^{\mathcal{N}}]-1\right)P_l(\cos\theta)\,,$$

where

$$f_c(\theta) = -\eta\{\exp[-2i\eta\log(\sin(\theta/2)) + 2i\,\delta_{0c}]\}/(2k\sin(\theta/2))\,,$$

$$\partial_l^c = \arg\Gamma(l+1+i\eta)\,,$$

$$2i\partial_l^{\mathcal{N}} = i\chi_{\mathrm{AB}} = -\tfrac{1}{2}\sigma_{\mathrm{tot}}(1-ia)\,AB\int \varrho_{\mathrm{A}}\,\varrho_{\mathrm{B}}\,\mathrm{d}^3\boldsymbol{r}\,,$$

$$(l+\tfrac{1}{2})k^{-1} = b\,, \qquad k = (2\mu^2 M_{\mathrm{A}}^{-1} E_{\mathrm{A}}^{\mathrm{lab}})^{\frac{1}{2}}\,, \qquad \mu = M_{\mathrm{A}}M_{\mathrm{B}}(M_{\mathrm{A}}+M_{\mathrm{B}})^{-1}\,.$$

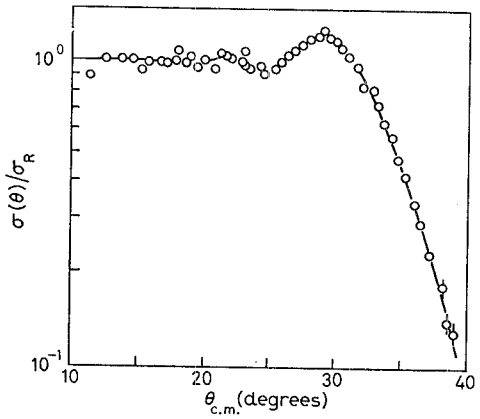

Fig. 4.5. – Elastic scattering od ^{16}O on ^{208}Pb (ref. [4.2]) at 158 MeV; the equivalent energy per nucleon is 4 MeV, $\sigma_{\mathrm{exp}}^{\mathcal{N}\mathcal{N}} = 2400$ mb, $\sigma_{\mathrm{th}}^{\mathcal{N}\mathcal{N}} = 2340$ mb.

The only parameters needed in the calculations are thus $\sigma^{\mathcal{N}\mathcal{N}}$, α and the parameters of the nuclear density distribution. The variation with energy of the elementary, free nucleon-nucleon total cross-section σ_{tot} is accounted for in the following way. σ_{tot} depends on the relative velocity ϑ_R of the colliding ions, which nonrelativistically can be found from the centre-of-mass relative energy. The last energy can be estimated by subtracting from the total centre-

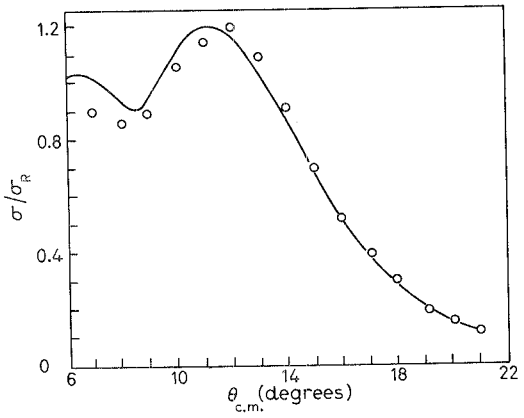

Fig. 4.6. – Elastic scattering of ^{16}O on ^{39}Ni (ref. [4.2]) at 158 MeV; the equivalent energy per nucleon is 7.2 MeV, $\sigma_{exp}^{\mathcal{N}\mathcal{N}} = 1300$ mb, $\sigma_{th}^{\mathcal{N}\mathcal{N}} = 1500$ mb.

of-mass energy the Coulomb energy, corresponding to the grazing collisions, when the distance between the centres of ions is equal to the sum of their radii. Thus σ_{tot} has to be taken at this nucleon energy E_{nuc}, which is evaluated from

$$E_{nuc} = \tfrac{1}{2} m \vartheta_R^2 ,$$

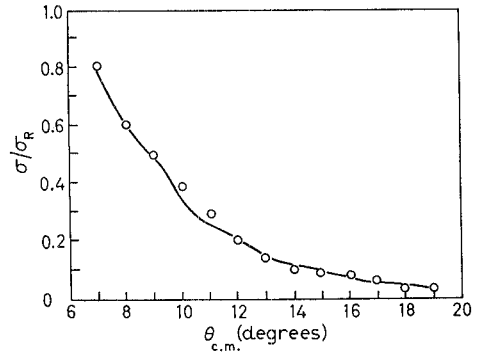

Fig. 4.7. – Elastic scattering of ^{16}O on ^{27}Al (ref. [4.2]) at 158 MeV; the equivalent energy per nucleon is 8.4 MeV, $\sigma_{exp}^{\mathcal{N}\mathcal{N}} = 1200$ mb, $\sigma_{th}^{\mathcal{N}\mathcal{N}} = 1290$ mb.

where

$$\vartheta_R^2 = \frac{2T_R}{\mu} = E_{c.m.} - \frac{Z_1 Z_2 e^2}{R_A + R_B} = \frac{l(l+1)\hbar^2}{2\mu(R_A + R_B)^2}.$$

The nucleon-nucleon total cross σ_{tot} is taken as $(1/2)(\sigma_{pn} + \sigma_{pp})$.

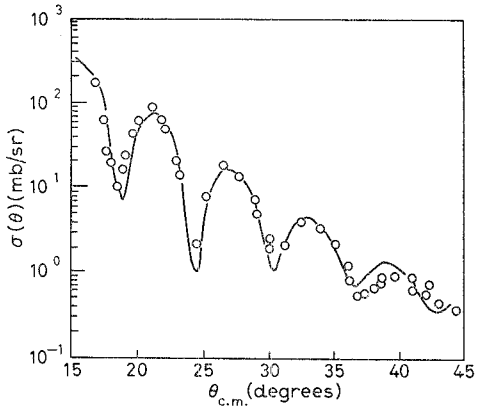

Fig 4.8. – Elastic scattering of ^{16}O on ^{12}C (ref. [4.2]) at 168 MeV; the equivalent energy per nucleon is 9.8 MeV, $\sigma_{exp}^{\mathcal{N}\mathcal{N}} = 1050$ mb, $\sigma_{th}^{\mathcal{N}\mathcal{N}} = 760$ mb.

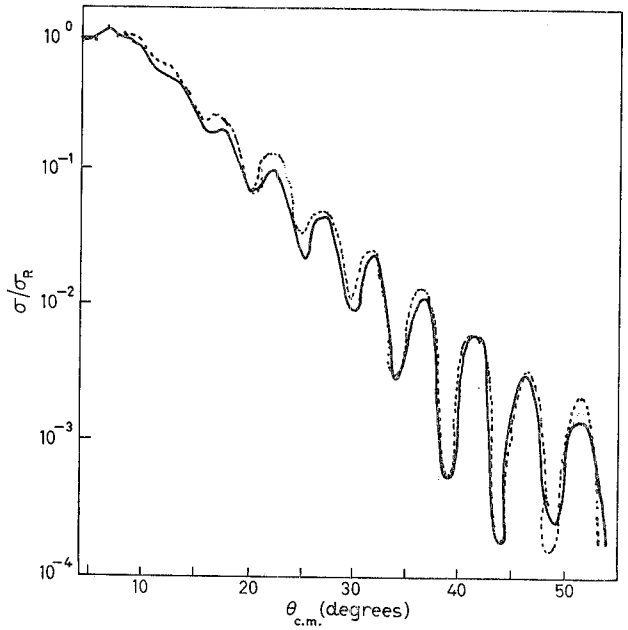

Fig. 4.9. – Elastic scattering of α-particles of ^{208}Pb (ref. [4.2]) at 104 MeV; the equivalent energy per nucleon is 18 MeV, $\sigma_{exp}^{\mathcal{N}\mathcal{N}} = 530$ mb, $\sigma_{th}^{\mathcal{N}\mathcal{N}} = 500$ mb (dashed line) and 300 mb (full line).

A systematic search with a best-fit program has been done to find the « best values » for these parameters, both for a Saxon-Woods density and for a Gaussian density. The comparison between the theoretical curves and the experimental data, for a wide range of masses and energies, is presented in fig. 4.5-4.10.

It appears that the angular distributions in fig. 4.5-4.10 are well fitted with σ^{NN}, which is in significant agreement with the experimental nucleon total cross-section. The parameter α is, in general, higher than its experimental value. It may, however, be pointed out that the corrections of higher powers of the nuclear density, which should be added to the phase shift $\chi(b)$ in eq. (4.31), can be regarded as an effective correction to σ^{NN} and α.

As for the nuclear parameters, in the case of Saxon-Woods densities the fitted values of r_0 ($R = r_0 A^{\frac{1}{3}}$) fall in the range $(1.0 \div 1.2)$ fm (the lower limit

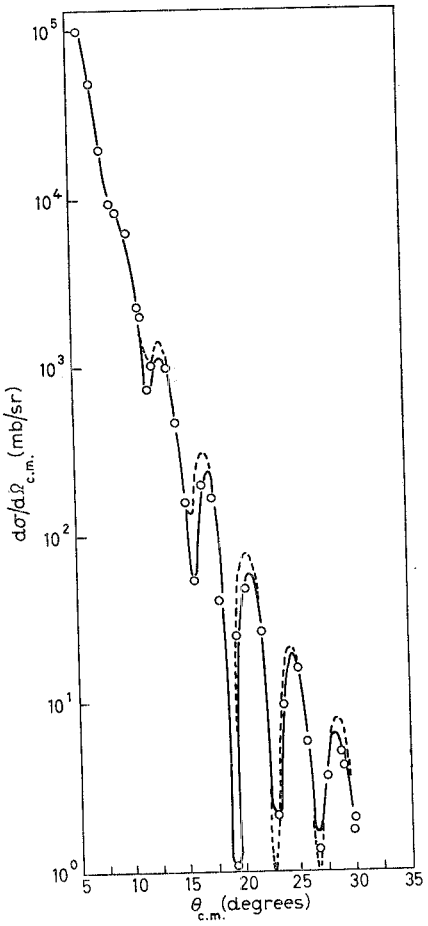

Fig. 4.10. – Elastic scattering of α-particles on ^{208}Pb (ref. [4.2]) at 166 MeV; the equivalent energy per nucleon is 34 MeV, $\sigma_{exp}^{NN} = 300$ mb, $\sigma_{th}^{NN} = 250$ mb (dashed line) and 224 mb (full line).

is in agreement with electron scattering data), and the fitted values for the diffuseness a take the values $(0.5 \div 0.65)$ fm.

Despite of various kinds of ambiguities in fixing the parameters, the comparison shown in fig. 4.5-4.10 demonstrates that the elastic scattering of heavy ions can be well reproduced (the greater energy the better) by means of the nuclear density and the free nucleon-nucleon total cross-section.

4.4 – Exact solution and eikonal correction.

The eikonal technique, which is simpler than the WKB method, may be extended both to larger angles and lower energies if it is combined with some known analytic solution, so that the eikonal method is used only for evaluating corrections arising from a small difference between the actual potential and the solvable one. This method was developed by BARTNIK, IWINSKI and one of the present authors [4.7] to deal with the screened Coulomb potential. We present this method in the case of the Coulomb potential, where it was tested, and indicate its extension to the case of a sum of nuclear and Coulomb potential. The last topic is currently investigated numerically.

For a Coulomb pointlike potential $V_C(r) = Z_p Z_t e^2/r$, we have

$$\begin{cases} \left(-\frac{\hbar^2}{2}\nabla^2 + V_C - E\right)\psi_c = 0\,, \\ \psi_c = \sqrt{\frac{\mu}{k}}\,\Gamma(1+i\eta)\exp\left[-\frac{\pi}{2}\eta\right]\exp\left[i\boldsymbol{k}\cdot\boldsymbol{r}\right]{}_1F_1(-i\eta;\,1;\,ik(r-z)) \end{cases} \tag{4.32}$$

with

$$k = (2\mu E)^{\frac{1}{2}}\,, \qquad \eta = Z_p Z_t e^2 \mu (\hbar k)^{-1}\,,$$

μ being the reduced mass of two ions.

For $V \neq V_C$, *e.g.* for a screened Coulomb field, we write the Schrödinger equation in the form

$$\left[-\frac{\hbar^2}{2\mu}\nabla^2 + V_C + (V - V_C) - E\right]\psi = 0 \tag{4.33}$$

and look for its solution in the form

$$\psi = f \exp\left[i\boldsymbol{k}\cdot\boldsymbol{r}\right]. \tag{4.34}$$

Thus f must satisfy the equation

$$[\nabla^2 + 2i\boldsymbol{k}\cdot\boldsymbol{\nabla} - 2\mu V_C - 2\mu(V - V_C)]f = 0 \tag{4.35}$$

and appropriate boundary conditions.

The essential point in the method of Bartnik *et al.* [4.7] is to replace eq. (4.35) by this 1st-order differential equation which by definition will reproduce the known result given by eq. (4.32) at all scattering angles and at all energies. It can be formally achieved by introducting a function f_c defined by

$$\psi_c \equiv f_c \exp[i\boldsymbol{k}\cdot\boldsymbol{r}] \tag{4.36}$$

and another function A which must satisfy the equation

$$(2i\boldsymbol{k}\cdot\boldsymbol{\nabla} - 2\mu V_C + A) f_c = 0 . \tag{4.37}$$

The same A is then used in an equation which replaces eq. (4.35). It is

$$[2i\boldsymbol{k}\cdot\boldsymbol{\nabla} - 2\mu V_C + A - 2\mu(V - V_C)] f = 0 , \tag{4.38}$$

and in contrast to eq. (4.35) it is very easy to solve. The solution of eq. (4.38) is

$$f = f_c f_1 , \tag{4.39}$$

where f_1 satisfies the equation

$$i\boldsymbol{k}\cdot\boldsymbol{\nabla} f_1 = \mu(V - V_C) f_1 , \tag{4.40}$$

thus it is simply given as

$$f_1 \sim \exp\left[-i\frac{\mu}{k}\int (V - V_C)\,\mathrm{d}z\right] \tag{4.41}$$

with the z-axis along the direction $\boldsymbol{k}$. It was found in ref. [4.7] that the solution of the whole problem written as $\psi = f_c f_1 \exp[i\boldsymbol{k}\cdot\boldsymbol{r}]$ satisfies the exact 2nd-order differential equation (4.35) with an accuracy better than 3 %, practically in the whole configuration space.

To apply the above method for evaluating differential cross-section for the elastic scattering of heavy ions, one must extend this method to include both the nuclear and Coulomb potentials. For two heavy ions the exact potential is taken as the square well in the inner region and the pointlike Coulomb potential in the outer region. We have

$$V_{\text{exact}} = \begin{cases} -V_0 & \text{for } r < a , \\ V_C & \text{for } r \geqslant a , \end{cases} \tag{4.42}$$

where a is a characteristic distance.

The ordinary 2nd-order Schrödinger equation is solved by taking the analytic solutions, in each partial wave, corresponding separately to the square well and V_C. Then, a sum over the partial-wave solutions, weighted with adjustable constants, is replaced by the impact parameter integral, which in turn is evaluated by the stationary-phase method. Standard continuity condition of the logarithmic derivative is required at $r = a$, and in this way we find an approximate wave function which we denote as ψ_{exact} in analogy to the pure Coulomb case discussed above. Having explicitly this ψ_{exact}, we define f_{exact} by

$$\psi_{\text{exact}} = f_{\text{exact}} \exp[i\boldsymbol{k}\cdot\boldsymbol{r}] \tag{4.43}$$

and find the wave function for the actual potential

$$V = V_N + V_C \tag{4.44}$$

in the following form:

$$\psi = f_{\text{exact}} \exp\left[i\boldsymbol{k}\cdot\boldsymbol{r} - i\frac{\mu}{k}\int_{\infty}^{z}(V_N + V_C - V_{\text{exact}})\,\mathrm{d}\zeta\right]. \tag{4.45}$$

The scattering amplitude is then calculated from the t-matrix element found by a numerical integration of ψ with V and a plane wave:

$$\begin{aligned}\langle k'|t|k\rangle = \langle \boldsymbol{k}'|V_N + V_C|\psi\rangle &= (2\pi)^{-3}\int \mathrm{d}^3r\,[V_N(r) + V_C(r)]\,f_{\text{exact}}\cdot \\ &\cdot\exp\left[i(\boldsymbol{k}-\boldsymbol{k}')\cdot\boldsymbol{r} - i\frac{\mu}{k}\int_{-\infty}^{z}(V_N + V_C - V_{\text{excat}})\,\mathrm{d}\zeta\right] = \\ &= (2\pi)^{-2}\int \mathrm{d}z\, b\,\mathrm{d}b\, J_0(b|\boldsymbol{k}-\boldsymbol{k}'|_\perp)\left[V_N\left(\sqrt{b^2+z^2}\right) + V_C\left(\sqrt{b^2+z^2}\right)\right] f_{\text{exact}}\cdot \\ &\cdot\exp\left[i(k_\parallel - k'_\parallel)\,z - i\frac{\mu}{k}\int_{-\infty}^{z}(V_N + V_C - V_{\text{exact}})\,\mathrm{d}\zeta\right],\end{aligned} \tag{4.46}$$

where $(\boldsymbol{k}-\boldsymbol{k}')_\perp$ and $k_\parallel - k'_\parallel$ denote the components of momentum transfer perpendicular and parallel to the chosen eikonal direction, respectively.

The impact parameter integral in eq. (4.46) should be evaluated by the method of stationary phase, while the remaining integrals, over J and Z, should be done numerically. This should be more efficient than the numerical solution of the Schrödinger equation for each partial wave. The advantage of our method should manifest itself especially at the medium and high energies, where the number of partial waves is very large indeed.

REFERENCES

[4.1] R. J. GLAUBER: in *Lectures in Theoretical Physics*, edited by W. E. BRITTIN Vol. **1** (New York, N. Y., 1959), p. 315; in *High-Energy Physics and Nuclear Structure*, edited by S. DEVONS (New York, N. Y., 1970), p. 207.
[4.2] A. DAR and Z. KIRZON: *Phys. Lett.*, **37** B, 166 (1971); *Nucl. Phys.*, **237** A, 319 (1975).
[4.3] T. W. DONNELLY, J. DUBACH and J. D. WALECKA: *Nucl. Phys.*, **232** A, 355 (1974).
[4.4] E. KUJAWSKI: *Phys. Rev. C*, **6**, 709 (1972).
[4.5] P. C. SABATIER: *Nuovo Cimento*, **37**, 1180 (1965).
[4.6] W. CZYZ and L. C. MAXIMON: *Ann. of Phys.*, **52**, 59 (1969).
[4.7] E. A. BARTNIK, Z. R. IWINSKI and J. M. NAMYSŁOWSKI: *Phys. Lett.*, **53** A, 5 (1975); *Phys. Rev. A*, **12**, 1785 (1975).

CHAPTER 5

Eikonal technique for inelastic scattering and transfer reactions.

5.1. – Coulomb excitation.

The simplest inelastic process is the Coulomb excitation. Only the energy is transferred to the target in this process, and the interaction potential responsible for excitation is the well-known Coulomb potential. There exist programs which allow for the numerical evaluation of Coulomb-excitation cross-section within the classical, or semi-classical or quantal scheme based on the DWBA method. Although the agreement of results evaluated from these programs and the experimental data is satisfactory, the numerical routines are very lengthy and preclude any insight into the formulae. GOLDFARB and one of the present authors [5.1] applied the eikonal technique to get an analytic expression for Coulomb excitation and in this way to gain some understanding of its dynamics. In particular, they looked at the role played by the nuclear moments in the expression for the transition matrix element.

Three points must be noted before discussing the final result:

a) most of the data for the Coulomb-excitation process is concentrated at large scattering angles, because in the forward direction the Rutherford scattering dominates the yield;

b) the Coulomb-excitation process is an inelastic one, and it may be associated with some features of an off-energy-shell t-matrix element with a shift of energy corresponding to the excitation energy;

c) for energies below the Coulomb barrier the DWBA scheme is quite adequate, and both the Coulomb distorted eigenfunctions and the interaction Hamiltonian causing the transition are well known.

Because of the first point one must deal with such an eikonal scheme which would give good results for large scattering angles. Luckily enough in the case of a pointlike Coulomb potential, approximated as a limiting case of the Yukawa potential,

$$V_C(r) = \lim_{\beta \to 0} \exp[-\beta r] \frac{Z_p Z_t e^2}{r}, \tag{5.1}$$

one can show that, by choosing our eikonal direction along the mean value of the initial and final relative momentum $\boldsymbol{\varkappa} = \frac{1}{2}(\boldsymbol{k}_i + \boldsymbol{k}_f)$ and defining the eikonal propagator with a pole depending in a special way on the scattering angle, namely

$$\tilde{G}_0 = m^{-1}(2mE)^{\frac{1}{2}} \left[p_\parallel - (2mE)^{\frac{1}{2}} \cos\frac{\theta}{2} - i\varepsilon \right]^{-1}, \tag{5.2}$$

it holds that the eikonal t-matrix $\tilde{t}$ defined as

$$\tilde{t} = -(2\pi)^2 m \langle \boldsymbol{k}_f | V_C - V_C \tilde{G}_0 V_C + V_C \tilde{G}_0 V_C \tilde{G}_0 V_C - \ldots | \boldsymbol{k}_i \rangle, \tag{5.3}$$

considered on the energy shell, coincides with the exact on-shell scattering t-matrix. It is most important that the agreement holds for an arbitrary scattering angle and an arbitrary energy.

Coming to the 2nd point we note that there exists an exact expression for the half-off-shell Coulomb t-matrix. Considering the case $|\boldsymbol{k}_f| < |\boldsymbol{k}_i|$, *i.e.* the one interesting for the Coulomb excitation, we write the result of Ford [5.2]

$$t_{\text{exact}}^{\text{half-shell}} = -2(2\pi\eta_i)^{\frac{1}{2}} k_i \eta_i |\boldsymbol{k}_i - \boldsymbol{k}_f|^{-2} \{(k_i^2 - k_f^2)|\boldsymbol{k}_i - \boldsymbol{k}_f|^{-2}\}^{i\eta_i} \cdot \exp\left[\frac{i\pi}{4} + i\eta_i \ln(\eta_i e^{-1})\right], \tag{5.4}$$

where η_i is the Sommerfeld parameter with $k = |\boldsymbol{k}_i|$.

The exact half-off-shell Coulomb t-matrix may be reproduced in the eikonal scheme if we choose a new eikonal direction and also consider heavy ions, so that $\eta_i, \eta_f \gg 1$. For large values of the Sommerfeld parameter one can analytically evaluate a first derivative with respect to the charge of the target, of the half-off-shell eikonal t-matrix. By denoting by ϱ the ratio of the magnitude of the parallel component of momentum transfer to the perpendicular component,

$$\varrho = |k_{f_\parallel} - k_{i_\parallel}| \cdot |\boldsymbol{k}_{f_\perp} - \boldsymbol{k}_{i_\perp}|^{-1}, \tag{5.5}$$

where $\|$ is along the eikonal direction, one can find

$$\frac{\partial}{\partial z_t} t_{\text{eikonal}}^{\text{half-shell}} = 2ik_i\eta_i Z_t^{-1}(\pi\eta_i)^{\frac{1}{2}} |\boldsymbol{k}_i - \boldsymbol{k}_f|^{-2-2i\eta_i}(\varrho^{-\frac{1}{2}} + i\varrho^{\frac{1}{2}}) \cdot \cdot \exp\left[-2\eta_i \operatorname{tg}^{-1}\varrho + 2i\eta_i \ln(2\eta_i e^{-1})\right].$$

The direction $\|$, *i.e.* the magnitude of ϱ, is fixed by the requirement

$$\left|\frac{\partial}{\partial z_t} t_{\text{eikonal}}^{\text{half-shell}}\right| = \left|\frac{\partial}{\partial z_t} t_{\text{exact}}^{\text{half-shell}}\right|. \tag{5.6}$$

It gives ϱ as the solution of the following transcendental equation:

$$(1+\varrho^2)\varrho^{-1}\exp\left[-4\eta_i \operatorname{tg}^{-1}\varrho\right] = 2\eta_i^2 \ln^2\left[\eta_i(k_i^2 - k_f^2)|\boldsymbol{k}_i - \boldsymbol{k}_f|^{-2}\right]. \tag{5.7}$$

Finally, we come to the 3rd point and consider the Coulomb excitation process within the DWBA scheme. Let us denote the relative position variable between a pointlike projectile and the centre of target by $\boldsymbol{r}$ and a variable denoting position of distributed charge in an extended target by $\boldsymbol{r}_p$. Then the interaction Hamiltonian describing the relative motion of the projectile in the field of charged target nucleus is

$$H = Z_t e^2 |\boldsymbol{r}_p - \boldsymbol{r}|^{-1} = Z_t e^2 r^{-1} + Z_t e^2[|\boldsymbol{r}_p - \boldsymbol{r}|^{-1} - r^{-1}]. \tag{5.8}$$

This splitting of the Hamiltonian into the first part which generates the distorted-wave eigenfunctions and into the residual part, depending explicitly on r_p, is characteristic of the DWBA procedure.

The Coulomb-excitation transition amplitude is given by the matrix element evaluated between the target nuclear states of a Coulomb distorted amplitude. More explicitly, we have

$$T_{fi}^{\text{Coulomb excitation}} = \langle\varphi_f(\boldsymbol{r}_p)|t_{fi}^{\text{DWBA}}(\boldsymbol{r}_p)|\varphi_i(\boldsymbol{r}_p)\rangle, \tag{5.9}$$

where $|\varphi_i(\boldsymbol{r}_p)\rangle$, $|\varphi_f(\boldsymbol{r}_p)\rangle$ are the target states, and

$$t_{fi}^{\text{DWBA}}(\boldsymbol{r}_p) = -(2\pi)^2 m\langle\chi_C(\boldsymbol{k}_f, \boldsymbol{r})|Z_t e^2|\boldsymbol{r}_p - \boldsymbol{r}|^{-1} - Z_t e^2 r^{-1}|\chi_C(\boldsymbol{k}_i, \boldsymbol{r})\rangle \tag{5.10}$$

with $\chi_C(\boldsymbol{k}_f, \boldsymbol{r})$ and $\chi_C(\boldsymbol{k}_i, \boldsymbol{r})$ denoting the Coulomb distorted waves.

We write

$$V_{r_p} = Z_t e^2 |\boldsymbol{r}_p - \boldsymbol{r}|^{-1}, \qquad V = Z_t e^2 r^{-1}, \tag{5.11}$$

and evaluate $t_{fi}^{\text{DWBA}}(\boldsymbol{r}_p)$ in the eikonal framework splitting it into four parts:

$$t_{fi}^{\text{DWBA}}(\boldsymbol{r}_p) = t^{(1)}(\boldsymbol{r}_p) - t^{(1)} + t^{(2)}(\boldsymbol{r}_p) - t^{(2)}, \tag{5.12}$$

where

$$t^{(1)}(\boldsymbol{r}_p) = -(2\pi)^2 m\langle \boldsymbol{k}_f|V_{r_p}(1-\tilde{G}_0^{(i)}V+\tilde{G}_0^{(i)}V\tilde{G}_0^{(i)}V-\ldots)|\boldsymbol{k}_i\rangle,$$

$$t^{(1)} = -(2\pi)^2 m\langle \boldsymbol{k}_f|V(1-\tilde{G}_0^{(i)}V+\tilde{G}_0^{(i)}V\tilde{G}_0^{(i)}V-\ldots)|\boldsymbol{k}_i\rangle,$$

$$t^{(2)}(\boldsymbol{r}_p) = -(2\pi)^2 m\langle \boldsymbol{k}_f|V(-\tilde{G}_0^{(f)}+\tilde{G}_0^{(f)}V\tilde{G}_0^{(f)}-\ldots)\,V_{r_p}(1-\tilde{G}_0^{(i)}V+\tilde{G}_0^{(i)}V\tilde{G}_0^{(i)}V-\ldots)|\boldsymbol{k}_i\rangle,$$

$$t^{(2)} = -(2\pi)^2 m\langle \boldsymbol{k}_f|V(-\tilde{G}_0^{(f)}+\tilde{G}_0^{(f)}V\tilde{G}_0^{(f)}-\ldots)\,V(1-\tilde{G}_0^{(i)}V+\tilde{G}_0^{(i)}V\tilde{G}_0^{(i)}V-\ldots|)\boldsymbol{k}_i\rangle$$

with $\tilde{G}_0^{(i)}$, $\tilde{G}_0^{(f)}$ corresponding to the initial and final energy, respectively. $t^{(1)}$ and $t^{(2)}$ are essentially the half-off-shell t-matrices which were considered in the 2nd point. $t^{(1)}(\boldsymbol{r}_p)$ and $t^{(2)}(\boldsymbol{r}_p)$ are similar quantities, but, because of the appearance of V_{r_p}, they require evaluation of slightly modified impact parameter integrals rather than these which are needed for $t^{(1)}$ and $t^{(2)}$. For example, we have

$$\frac{\partial}{\partial z_t}t^{(1)}(\boldsymbol{r}_p) = -2\eta_i k_i Z_t^{-1}\exp[-ir_\parallel\delta]\cdot \cdot\int_0^\infty db\, bJ_0(b\Delta)K_0[(b^2+s^2-2bs\cos\varphi)\delta]b^{2i\eta_i} \tag{5.13}$$

with

$$r_\parallel = \boldsymbol{r}_p\cdot\boldsymbol{k}k^{-1}, \qquad \delta = k_{f_\parallel}-k_{i_\parallel} = \varrho(1+\varrho^2)^{-\frac{1}{2}}|\boldsymbol{k}_f-\boldsymbol{k}_i|, \qquad \boldsymbol{s}\equiv(\boldsymbol{r}_p)_\perp,$$

φ the angle between $r_{p\perp}$ and $(\boldsymbol{k}_f-\boldsymbol{k}_i)_\perp$ and $\Delta = |\boldsymbol{k}_f-\boldsymbol{k}_i|_\perp$.

It can be shown that for large values of the Sommerfeld parameter the final result for the integral in eq. (5.13) is similar to the corresponding one for $t^{(1}$ and can be obtained from the latter one by the substitution

$$|\boldsymbol{k}_f-\boldsymbol{k}_i|^2 \to |\boldsymbol{k}_f-\boldsymbol{k}_i|^2[1-\varrho^2(1+\varrho^2)^{-1}\eta_i^{-1}\boldsymbol{r}_p\cdot(\boldsymbol{k}_f-\boldsymbol{k}_i)_\perp]. \tag{5.14}$$

However, for large $\eta\gg1$, φ is very small and with a good approximation may be neglected in eq. (5.14). The main dependence on $\boldsymbol{r}_p$ then remains in eq. (5.13) in the factor $\exp[-ir_\parallel\delta]$. This factor is expanded in the power series

$$\exp[-ir_\parallel\delta] = \sum_L(-ir_\parallel\delta)^L(L!)^{-1}, \tag{5.15}$$

and a specific transition with multipolarity L is weighted by δ^L. The powers of $r_\parallel\delta$ can be better understood if we write

$$r_\parallel\delta = r_\parallel(k_{f_\parallel}-k_{i_\parallel}) = \left(\frac{4}{3}\pi\right)^{\frac{1}{2}} r_p\varrho(1+\varrho^2)^{-\frac{1}{2}}|\boldsymbol{k}_f-\boldsymbol{k}_i|\sum_m Y_{lm}^*\left(\frac{\boldsymbol{k}}{k}\right)Y_{lm}\left(\frac{\boldsymbol{r}_p}{r_p}\right). \tag{5.16}$$

Then, returning to eq. (5.9), we see that in the matrix element for Coulomb excitation there will be factors of the type

$$\langle \varphi_f(\boldsymbol{r}_p) | r_p^L Y_{LM}\left(\frac{\boldsymbol{r}_p}{r_p}\right) | \varphi_i(\boldsymbol{r}_p) \rangle \sim \sqrt{B(EL)} \,, \tag{5.17}$$

determined by the reduced transition probabilities of multipolarity L for the target nucleus. Numerical evaluations of the Coulomb excitation matrix elements for either α or ^{16}O scattered on ^{208}Pb are currently investigated by GOLDFARB and one of the present authors [5.1]. This method may be also extended to two-step processes and applied to the evaluation or reorientation effects.

5.2. – Transfer reactions in the DWBA scheme with the eikonal distorted waves.

Here we are considering heavy-ion transfer reactions well above the Coulomb barrier. The conventional DWBA calculations are very laborious because of very many partial waves and a simplification of the 6-dimensional DWBA integral by neglecting the recoil is forbidden, because recoil plays and essential role at higher energies, as was noted in chapter 3.

To simplify the DWBA codes at energies well above the Coulomb barrier DA SILVEIRA, GALIN and NGO [5.3] proposed to evaluate distorted waves in the eikonal approximation. In addition, they neglected recoil and assumed a localization approximation. These additional assumptions, especially the first one, should not be made at higher energies, but DA SILVEIRA *et al.* wanted to have simpler expressions to handle and on such expressions they tested their DWBA high-energy scheme. The formula for the nucleon transfer differential cross-section is the one proposed by BUTTLE and GOLDFARB [5.4] and given explicitly in chapter 3. Furthermore, DA SILVEIRA *et al.* assumed that for high incident energy the Q-value of the reaction is small compared to the energy, so they put $k_i \approx k_f \approx k$, and they disregarded differences between optical potentials in the initial and final channels, putting

$$V^i_{opt}(r_i) \approx V^f_{opt}(r_f) = \overline{V}_{opt}(r) \,. \tag{5.18}$$

Then, the product of the initial and final distorted waves is calculated in the eikonal scheme:

$$\chi^{(+)}(\boldsymbol{k}_i, \boldsymbol{r})\, \chi^{(-)*}(\boldsymbol{k}_f, \boldsymbol{r}) \approx \exp\left[i\boldsymbol{q}\cdot\boldsymbol{b} - i(\hbar v)^{-1} \int_{-\infty}^{\infty} \overline{V}_{opt}(r)\, \mathrm{d}z' \right], \tag{5.19}$$

where $|\boldsymbol{q}| = 2k \sin(\theta/2)$ and $\boldsymbol{b}$ is connected with $\boldsymbol{r}$ by $\boldsymbol{r} = \boldsymbol{b} + \boldsymbol{k}k^{-1}z$.

The simplification achieved on the r.h.s. of eq. (5.19) enables us to write an expression on $T_{l\lambda}(\theta)$ defined in chapter 3 in the form of a one-dimensional impact parameter integral:

$$T_{l\lambda}(\theta) \approx Y_{l\lambda}\left(\frac{\pi}{2}, 0\right) \int_0^\infty \mathrm{d}b\, b J_\lambda(qb) K_0\left(\sqrt{2mB_2\hbar^{-2}}\, b\right) n(b) \tag{5.20}$$

with

$$n(b) = \exp\left[-i(\hbar v)^{-1} \int_{-\infty}^{\infty} \overline{V}_{\mathrm{opt}}(r)\, \mathrm{d}z\right], \qquad l + \lambda \text{ even},$$

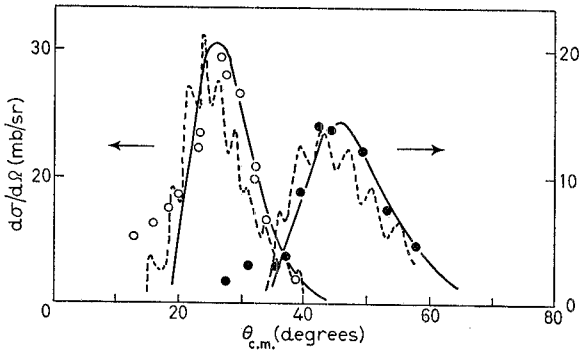

Fig. 5.1. – Neutron pick-up reaction at 78 (•) and 113 MeV (○). The curves are the result of theoretical calculations using two shapes: square (dashed curve) and Saxon-Woods (full curve), ref. [5.3]. Experimental data are from ref. [5.5]. (^{14}N on Ag) $^{14}\mathrm{N} \rightarrow \mathrm{ln} + {}^{15}\mathrm{N}$.

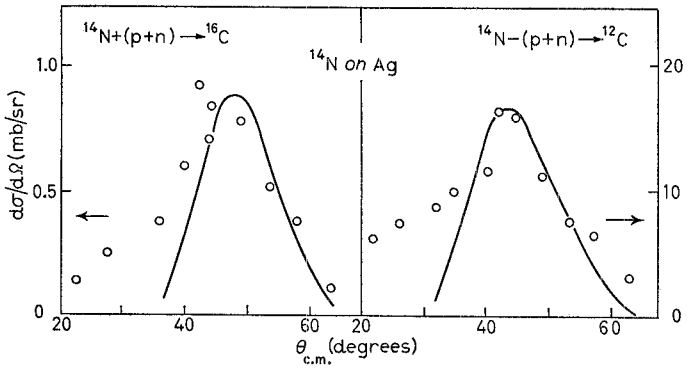

Fig. 5.2. – Two-nucleon (proton and neutron) transfer reaction: pick-up (l.h.s.) and stripping (r.h.s.). The curves are the result of theoretical calculations using a Saxon-Woods potential, ref. [5.3], experimental data are from ref. [5.5]. $E_{\mathrm{lab}} = 78$ MeV.

and J_λ, K_0 are cylindrical and second-order Bessel functions. Taking advantage of the localization approximation, one can use an asymptotic behaviour of K_0 and put in (5.20)

$$K_0(\sqrt{2mB_2\hbar^{-2}}\,b) \simeq \left[\exp\left[-\sqrt{2mB_2\hbar^{-2}}\,b\right]\right] b^{-\frac{1}{2}}. \tag{5.21}$$

In fig. 5.1 and 5.2 we show the results of Da Silveira *et al.* [5.3] for the transfer reactions induced by the ^{14}N projectiles on the Ag target. The distorting optical potential was found by fitting the elastic-scattering data; various forms of the nuclear part of the potential were tried. As is seen, apart from the region of small angles, the agreement between theory and experiment is quite good.

5.3. – Heavy-ion transfer reactions in an eikonal scheme, without DWBA.

The formalism presented in this section is an extension to the transfer reactions of the scheme described in **4.4**. It is currently investigated numerically, thus we shall give only the main formulae and state our motivations.

Our aims are

a) to include a 3-body description in transfer processes $(c_1, t) + c_2 \to c_1 + (c_2, t)$, where the three « bodies » are c_1, c_2 and t (see fig. 3.6)

b) to include recoil and most of the 3-body kinematics, except for the internal motion in the target;

c) to avoid a partial-wave expansion in the relative motion of ions by introducing the impact parameter representation;

d) to benefit from the simplicity of the eikonal formalism, but in such a form that it works for an arbitrary scattering angle and energy, *i.e.* to use the eikonal formalism only for the evaluation of a correction to the exact, analytic solution.

These aims are realized by starting from the definition of the 3-body transition operators. It is useful, and a common practice among people doing 3-body calculations, to denote the three particles and the three possible 2-body bound states by the same indices α, β, γ. Thus the particle α, like c_2, is approaching the bound state $(\beta, \gamma) = \alpha$, like (c_1, t), and in the final-state particle β emerges, like c_1, and the bound state $(\alpha, \gamma) = \beta$, like (c_2, t).

Then, if 2-body interactions between the three pairs are denoted as V_α, V_β, V_γ, corresponding to the pairs (β, γ), (α, γ) and (α, β), respectively, and

$$\overline{V}_{\alpha,\beta} = V - V_{\alpha,\beta}, \qquad V = \sum_{\alpha=1}^{3} V_\alpha, \tag{5.22}$$

the 3-body transition operator describing the process

$$\alpha + (\beta, \gamma) \to \beta + (\alpha, \gamma)$$

is

$$T_{\beta\alpha} = \langle \phi_\beta | \overline{V}_\beta | \psi_\alpha^{(+)} \rangle = \langle \psi_\beta^{(-)} | \overline{V}_\alpha | \phi_\alpha \rangle , \tag{5.23}$$

where $\phi_{\alpha,\beta}$ are the channel wave functions in the initial, final state made out of a plane wave associated with α, β, respectively, and the bound-state wave functions (β, γ) and (α, γ) correspondingly, and $\psi_{\alpha,\beta}$ are the wave functions corresponding to the interaction in the initial, final state, respectively.

To evaluate the 3-body scattering wave function $\psi_\alpha^{(+)}$ for example in the channel corresponding to $c_1 + (c_2, t)$, we suggest the following procedure. Introduce the notation $\boldsymbol{r}$ and $\boldsymbol{R}$ for the relative positions between the $c_1 c_2$ cores, and between the transferred particle t and the centre-of-mass system of the (c_1, c_2) subsystem, respectively. The three potentials between t, c_1 and c_2 are written in the notation as

$$\begin{cases} V_{tc_1}\left(-\dfrac{m_2}{m_1+m_2}\boldsymbol{r} - \boldsymbol{R}\right), \\ V_{tc_2}\left(\dfrac{m_1 \boldsymbol{r}}{m_1+m_2} + R\right), \\ V_{c_1c_2}(\boldsymbol{r}) = V_{c_1c_2}^{\text{Coulomb}} + V_{c_1c_2}^{\text{Coulomb}}. \end{cases} \tag{5.24}$$

Next consider two auxiliary, separate, 2-body–like problems

$$[-\tfrac{1}{2}\mu^{-1}\Delta_R^2 + V_{tc_1}(-\boldsymbol{R}) + V_{tc_2}(\boldsymbol{R})]\,\chi(\boldsymbol{R}) = \varepsilon\chi(\boldsymbol{R}), \tag{5.25a}$$

$$[-\tfrac{1}{2}\nu^{-1}\Delta_r^2 + V_{c_1c_2}^{\text{Coulomb}}(\boldsymbol{r})]\,\chi(\boldsymbol{r}) = (E-\varepsilon)\,\chi(\boldsymbol{r}), \tag{5.25b}$$

where $\nu = m_1 m_2 (m_1+m_2)^{-1}$, $\mu = m_t(m_1+m_2)(m_1+m_2+m_t)^{-1}$.

To each of the above equations we apply separately the method given in sect. 4.4, and denote the analogs of the function A, appearing in eq. (4.38), as a and b, for eqs. (5.25a) and (5.25b), respectively. Then we solve analytically a linearized 3-body Schrödinger equation, in which both operators Δ_R^2 and Δ_r^2 are replaced by the respective 1st-order differential operators, and the functions a and b. In this 3-body, linearized equation we put the full potentials, as they are written in eq. (5.24). The functions a and b can be eliminated in the found solution in a similar way as it in sect. 4.4. Finally, the initial condition, corresponding to the channel $c_1 + (c_2, t)$ is built in by using the Lippmann-Schwinger equation in this channel. However, instead of solving the Lippmann-Schwinger equation, we put on the r.h.s. of it the scattering wave function obtained

from the linearized 3-body Schödinger equation, as described above. Through the quasi–2-body free Green's function in the Lippmann-Schwinger equation we take into account the initial condition in the $c_1 + (c_2, t)$ channel.

To evaluate the matrix elements in eq. (5.23) we use the stationary-phase method in the impact parameter integrals, and evaluate numerically only the integrals corresponding to the direction orthogonal to the impact parameter plane. An application of this method to treat simultaneously the elastic-scattering and transfer reactions with the use of the same potentials written in eq. (5.24) is currently investigated for one- and two-nucleon heavy-ion transfer reactions and the corresponding elastic channels.

5.4. – Faddeev-Lovelace equations in the eikonal approximation.

Finally, we come to an eikonal scheme in which one does not write the solution for transition operators, but integral equations for these quantities. Such a scheme can incorporate 3-body dynamical effects in all possible configurations, without some approximations which were needed in sect. **5.3**. However, this is done at the expense of solving integral equations. The eikonal technique serves two purposes. First, to simplify the Green's function, second, to by-pass partial-wave expansion.

To make this program more definite we briefly mention the work of Janev and Salin [5.6], where a nonstationary scattering theory was used together with the straight-line eikonal approximation. The channel wave functions are taken as

$$(5.26) \qquad \begin{cases} \tilde{\Phi}_\alpha = \varphi_\alpha(\boldsymbol{x}) \exp\left[-iE_\alpha t - ip\boldsymbol{v}\cdot\boldsymbol{r} - i(2m_3)^{-1}p^2v^2t\right], \\ \tilde{\Phi}_\beta = \varphi_\beta(\boldsymbol{s}) \exp\left[-iE_\beta t + iq\boldsymbol{v}\cdot\boldsymbol{r} - i(2m_3)^{-1}q^2v^2t\right] \end{cases}$$

with $\boldsymbol{x} = \boldsymbol{r}_{32}$, $\boldsymbol{s} = \boldsymbol{r}_{31}$, $\boldsymbol{r}_{ij} = \boldsymbol{r}_i - \boldsymbol{r}_j$, $p = m_1m_3/(m_1+m_2)$, $q = m_2m_3/(m_1+m_2)$, $\boldsymbol{v}$ the relative velocity of the incoming particle and the target in the initial channel, $\varphi_\alpha(\boldsymbol{x})$, $\varphi_\beta(\boldsymbol{s})$ the eigenfunctions for the bound states of particles $(1 + 3)$ and $(2 + 3)$, respectively, and $E_{\alpha,\beta}$ the corresponding eigenenergies. In the straight-line eikonal approximation we have

$$\boldsymbol{r} = \boldsymbol{r}(t) = \boldsymbol{b} + \boldsymbol{v}t,$$

where t denotes time.

JANEW and SALIN defined appropriate 3-body transition operators and wrote the Faddeev-Lovelace integral equations for these operators. The structure of these equations is similar to the standard 3-body equations, however an important simplification, caused by the eikonal approximation, is the reduction of dimensions of integration from 6 to $3 + 1$. A by-product of the work

of Janev and Salin is an explicit dependence on one potential of a transition operator evaluated in the approximation when only two of the potentials are kept and one is set equal to zero. The whole influence of the 3rd potential reduces merely to a phase factor

$$\exp\left[-i\int_{-\infty}^{+\infty} V_3(t)\,\mathrm{d}t\right].$$

This is an important result in connection with our discussion in the previous section, where one of the interactions was only partially included in the wave function over which the processes (5.24) were averaged.

* * *

One of the Authors (JMN) would like to acknowledge Prof. G. BELLETTINI for a kind invitation and hospitality at the Frascati National Laboratories.

REFERENCES

[5.1] L. J. B. GOLDFARB and J. M. NAMYSŁOWSKI: Manchester preprint (to be published).
[5.2] W. F. FORD: *Journ. Math. Phys.*, **7**, 626 (1966).
[5.3] R. DA SILVEIRA, J. GALIN and C. NGO: *Nucl. Phys.*, **159** A, 481 (1970).
[5.4] P. J. A. BUTTLE and L. J. B. GOLDFARB: *Nucl. Phys.*, **78**, 409 (1966).
[5.5] J. GALIN, D. GUERRAN, M. LEFORT, J. PETER and X. TARRAGO: *Nucl. Phys.*, **159** A, 461 (1970).
[5.6] R. K. JANEV and A. SALIN: *Ann. of Phys.*, **73**, 136 (1972).

PUBLISHED PAPERS

P. E. HODGSON – Nuclear heavy-ion reactions.

V. M. CANUTO – New trends in cosmology.

G. C. GHIRARDI, C. OMERO, A. RIMINI and T. WEBER – The stochastic interpretation of quantum mechanics: a critical review.

W. M. ALBERICO, B. CENNI and A. MOLINARI – The response function of the infinite nuclear matter.

Y. NE'EMAN and T. REGGE – Gauge theory of gravity and supergravity on a group manifold.

R. HAKIM – Statistical mechanics of relativistic dense matter.

M. FRANCAVIGLIA – Applications of infinite-dimensional differential geometry to general relativity.

F. W. BOPP – The cluster model.

G. GIAQUINTA and N. A. MANCINI – Superconducting order parameter fluctuations and pair tunnelling.

FORTHCOMING PAPERS (in alphabetical order)

A. BASSETTO – Many-hadron production at low $P_\perp$. Some ideas collected and framed into a hierarchy of upper bounds.

G. S. BISNOVATYI-KOGAN – Magnetohydrodynamical processes near compact objects.

S. V. GANTSEVICH, V. L. GUREVICH and R. KATILIUS – Theory of fluctuations in nonequilibrium electron gas.

H. HUSSEIN et V. GILLET – Techniques simplifiées pour les calculs du modèle en couches.

W. KUTSCHERA, B. A. BROWN and K. OGAWA – The empirical $(1f_{\frac{7}{2}})^n$ model.

L. SERTORIO – Statistical mechanics at high energy.

A. MAŁECKI, *et al.*
Rivista del Nuovo Cimento
Serie 3, Vol. 1, N. 10 - 1978